Université Mohamed Khider de Biskra
Faculté des Sciences et de la Technologie
Département de génie électrique

MÉMOIRE DE MASTER

Sciences et Technologies
Filière : Electronique
Spécialité : Electronique des systèmes embarqués

Réf. : .....

Présenté et soutenu par :
Djemai Diana **Benatallah Amel**

Le : .....

Simulation SCAPS-1D de la cellule solaire à pérovskite MASnI3

Jury :

M.	Guesbaya Taher	MCA	Université de Biskra	Président
Mme.	Tobbeche Souad	Pr	Université de Biskra	Rapporteur
Mme.	Toumi Abida	Pr	Université de Biskra	Examinateur

Année universitaire : 2024 - 2025

Université Mohamed Khider de Biskra
Faculté des Sciences et de la Technologie
Département de génie électrique

MÉMOIRE DE MASTER

Sciences et Technologies
Filière : Electronique
Spécialité : Electronique des systèmes embarqués

Réf. : .....

Simulation SCAPS-1D de la cellule solaire à pérovskite MASnI3

Le : ……..

Présenté par :

Djemai Diana
Benatallah Amel

Avis favorable de l'encadreur :

Tobbeche Souad

Signature Avis favorable du Président du Jury

Guesbaya Taher

Cachet et signature

Mohamed Khider University of Biskra
Faculty of Science and Technology
Department of Electrical Engineering

MASTER'S THESIS

Science and Technology
Sector: Electronics
Specialty: Embedded systems electronics

Ref.:.....

Presented and supported by:
Djemai Diana **Benatallah Amel**

THE :.....

SCAPS-1D simulation of perovskite solar cell MASnI3

Jury:

Mr.	Guesbaya Taher	MCA	University of Biskra	President
Mme.	Tobbeche Souad	Pr	University of Biskra	Rapporteur
Mme.	Toumi Abida	Pr	University of Biskra	Examiner

Academic year:2024 - 2025

Mohamed Khider University of Biskra
Faculty of Science and Technology
Department of Electrical Engineering

MASTER'S THESIS

Science and Technology
Sector: Electronics
Specialty: Embedded systems electronics

Ref.:.....

SCAPS-1D simulation of perovskite solar cell MASnI3

THE :.....

Presented by:

Djemai Diana
Benatallah Amel

Favorable opinion from the supervisor:

Tobbeche Souad

Signature Favorable opinion of the President of the Jury

Guesbaya Taher

Stamp and signature

Dedication

To my dear parents, for all their sacrifices, their love, their tenderness, their support, and their prayers throughout my studies,

To my dear sisters Djihane, Yousra, Yassmine, and Hadda Nour for their constant encouragement and moral support,

To my dear brothers, Monib, for their support and encouragement,

To my uncle Mohammed and my aunts Aicha and Masseouda, I dedicate to you in gratitude for all their encouragement and moral support and as a token of my gratitude and affection,

To my friends Mohammed, Rawan and Reem for their moral support

To all those who are dear to me.

Djemai Diana

Dedication

I dedicate this work to the best parents, my father BENATALLH SADOK and HAMIDI HENIA and my virtuous husband Masmoudi soufiane, and my daughters meriem, mayar,Hidaya mebarka and manasa, and to my mother akrroum mebarka, and to my brothers and sisters, and also to all my family.

I would also like to thank all the professors. I would also like to thank my friends (Baia , Balqis, Nasreen and all members of the 2025 cohort...).

BenAtallh Amel

Acknowledgments

First of all, we thank Almighty God for giving us the will, health, and strength to complete this work.

We would like to thank Ms.TOBBECHE SOUAD for agreeing to supervise us, for directing this work, for his availability, his patience, and his valuable advice, which greatly contributed to the completion of this work.

We also thank Mr. GUESBAYA TAHER for having done us the honor of chairing this dissertation jury.

We also thank Ms. ABIDA TOUMI for agreeing to review this work.

Finally, we would like to express our gratitude to all those who enabled us to complete this work.

Djemai Diana

BenAtallah Amel

Abstract

This work involves the simulation and optimization of a photovoltaic solar cell based on the hybrid perovskite material $MASnI_3$, using the one-dimensional simulation tool SCAPS. The primary objective is to optimize the solar cell performance by determining optimal parameters, such as layer thicknesses and doping concentrations of the electron transport layer (ETL) and the hole transport layer (HTL). The results showed that the layer thicknesses that provide maximum electrical performance are 0.1 μm for Spiro-OMeTAD (HTL), 0.6 μm for $MASnI_3$, and 0.1 μm for CeOx (ETL). the optimal doping concentration are $10^{21}cm^{-3}$ for the Spiro-OMeTAD, and $10^{21}cm^{-3}$ for the CeOx. These optimizations yield the following photovoltaic performance: V_{CO} = 0.9029 V, Jsc = 34.57 mA/cm^2, FF = 80.45% and η = 25.11%. Additionally, the effects of defects in the perovskite layer, interfaces (perovskite/ETL and perovskite/HTL), and temperature variations were investigated. All these factors were found to reduce the solar cell's efficiency.

Résumé

Ce travail porte sur la simulation et l'optimisation d'une cellule solaire photovoltaïque basée sur le matériau hybride pérovskite $MASnI_3$, en utilisant l'outil de simulation unidimensionnel SCAPS. L'objectif principal est d'optimiser les performances de la cellule solaire en déterminant les paramètres optimaux, tels que les épaisseurs des couches et les concentrations de dopage de la couche de transport d'électrons (ETL) et de la couche de transport de trous (HTL). Les résultats ont montré que les épaisseurs de couches offrant les meilleures performances électriques sont de 0,1 µm pour le Spiro-OMeTAD (HTL), 0,6 µm pour le MASnI3 et 0,1 µm pour le CeOx (ETL). Les concentrations de dopage optimales sont de 10^{21} cm^{-3} pour le Spiro-OMeTAD et de 10^{21} cm^{-3} pour le CeOx. Ces optimisations permettent d'atteindre les performances photovoltaïques suivantes : V_{CO} = 0,9029 V, Jsc == 34,57 mA/cm², FF = 80,45 % et η = 25,11 %. De plus, les effets des défauts dans la couche de pérovskite, aux interfaces (pérovskite/ETL et pérovskite/HTL) ainsi que les variations de température ont été étudiés. Tous ces facteurs ont été trouvés comme ayant un impact négatif sur le rendement de la cellule solaire.

الملخص

يتضمن هذا العمل محاكاة وتحسين خلية شمسية كهروضوئية مبنية على مادة البيروفسكايت الهجينةMASnI3 ، باستخدام أداة المحاكاة أحادية البعد .SCAPS الهدف الرئيسي هو تحسين أداء الخلية الشمسية من خلال تحديد المعلمات المثلى، مثل سُمك الطبقة وتركيزات التشويب لطبقة نقل الإلكترون (ETL) وطبقة نقل الثقوب .(HTL) أظهرت النتائج أن سُمك الطبقة الذي يوفر أقصى أداء كهربائي هو 0.1 ميكرومتر لـ(Spiro-OMeTAD (HTL ، و0.6 ميكرومتر لـMASnI3 ، و0.1 ميكرومتر لـ .(CeOx (ETL تركيز التشويب الأمثل هو 1021 سم-3 لـ Spiro-OMeTAD، و1021 سم-3 لـ .CeOx أدت هذه التحسينات إلى تحقيق الأداء الكهروضوئي التالي:

V_{CO} = 0.9029 فولت، Jsc = 34.57 مللي أمبير/سم²، FF = 80.45%، η = 25.11%. بالإضافة إلى ذلك، تم دراسة آثار عيوب طبقة البيروفسكايت، والسطوح البينية (بيروفسكايت/ETL وبيروفسكايت/HTL)، وتغيرات درجة الحرارة. وقد وُجد أن جميع هذه العوامل تُقلل من كفاءة الخلية الشمسية.

List of figures

List of figures

Chapitre I

Chapitre II

Chapitre III

Chapitre IV

List of tables

List of tables

Chapitre I

Chapitre II

Chapitre IV

List of Symbols and Abbreviations

List of abbreviations

H	Planck's constant
C	Speed of light
λ	Wavelength of radiation in μm
ν	Radiation frequency
Ep	Photon energy
h	Planck's constant
I0	[Incident intensity [cm-1
A	[Absorption coefficient [cm
X	Penetration depth
I0	Saturation current
Q	Electron charge
K	Boltzmann's constant
T	Temperature
n	Diode ideality factor
V	(Position potential (V
Jcc ou Jsc	Short-circuit current density
Vco ou Voc	Open-circuit voltage
FF	Form factor FF
Pin	Incident light energy
Pmax	Maximum energy delivered by the cell
IQE	Quantum efficiency
Nph	Photon flux
ID	Diode reverse current
I0	Diode saturation current, temperature dependent
ILight	Photocurrent, irradiation intensity dependent Parallel
RSH	resistance
Rs	Series resistance
Vpv	Voltage across the cell
Ipv	Cell supplied current

m	Material index
k	Boltzmann constant
T	Temperature in Kelvin
q	Electron charge
PCE	Power conversion efficiency
HTL	Hole transport material
ETL	Electron transport material
Nt	Defect density
ND	(Doping concentration (donor
ISC	Short-circuit current
Voc	Open circuit voltage
FF	Form factor
η	Solar cell conversion efficiency
SCAPS	Solar Cell Capacitance Simulator one Dimension Plumb
TiO2	Copper oxide
PV	Photovoltaic
PSC	Power conversion efficiency
Pm	Maximum power
QE	Cell quantum efficiency
Rs	Series resistance
Rp	Shunt resistance
Iph	Photocurrent
CaTiO3	.Calcium titanate Structure of a generic perovskite crysta
ABX3	Methylammonium
CH3NH3I+= MA	Polythiophene
CH3NH3PbI3	Diffusion length
D	Diffusion coefficient
τ	Carrier lifetime
me	Affective mass
Au	Ore
Al	Aluminum

Ag	Silver
φ	Potential
q	Elementary charge
ε	Permittivity
N	Free electron density
p	Free hole density
ND	Donor doping density
NA	Acceptor doping density
pt	Hole trap density
nt	Electron trap density
Gn	Electron optical generation rate
Gp	Hole optical generation rate
Rn	Electron recombination rate
Rp	Hole recombination rate
Jn	Electron current density
Jp	Hole current density
μn	Electron mobility
μ**p**	Hole mobility
Dn	Electron diffusion coefficient
Dp	Hole diffusion coefficient
KB	Boltzmann constant
T	Temperature
Ln	Electron diffusion length Hole diffusion length
L**p**	Electron lifetime
τn	Hole lifetime
τ**p**	Effective density of states of the conduction band
NC	Effective density of states of the valence band
NV	Shockley-Read-Hall
SRH	Recombination coefficient
γ	Intrinsic concentration

ni	Equilibrium electron concentration.
n0	Equilibrium hole concentration
p0	Absorption coefficient
α	Work function
Φm	Electron affinity
χ	Light-generated current density
Jph	Saturation current in the dark
J0	Gap energy
Eg	Methylammonium tin triiodide
MA	(Poly(3,4-ethylenedioxythiophene
SnI3	Polystyrene sulfonate
PEDOT:PSS	Phenyl-C61-butyric acid methyl ester
PCBM	

Table of contents

Table of contents

Chapter II : The Perovskite Solar Cells

Chapter III : Presentation of the SCAPS-1D Software

General Introduction

General Introduction

In light of increasing environmental and economic challenges, there is an urgent need to develop clean, sustainable, and cost-effective energy sources. Solar energy is one of the most prominent of these sources, as it is renewable, abundant, and plays a pivotal role in reducing dependence on fossil fuels. Solar cells rely on the photovoltaic effect to convert light into electrical energy, a field that has witnessed significant development in recent years, particularly with the emergence of new generation solar cell technologies.

Among the most promising materials in this context are perovskites, which have attracted extensive research interest due to their unique properties, such as high absorption coefficient, excellent charge carrier mobility, and effective diffusion length. Their ability to be manufactured using low-cost techniques such as spraying, spin printing, and spin coating makes them a strong candidate to replace silicon in the near future.

Perovskite cells can be manufactured using multiple thin layers, precisely arranged for maximum efficiency. The traditional construction of these cells includes a transparent conductive layer as (FTO), a blocking layer (BOL), an electron transport layer (ETL), an active perovskite layer, followed by a hole transport layer (HTL), and finally a back contact. These layers are designed using a number of advanced nanomaterials, such as (CeOx) for electron transport and spiro-OMeTAD or for hole transport, depending on the cell's structural design.

However, despite the high efficiency achieved by perovskite cells in the laboratory, several challenges hinder their widespread commercialization, most notably chemical and thermal stability, the effect of humidity, and operational lifetime. This is where modeling and computer simulation tools become crucial, as they enable the study of the impact of structural and physical variables on cell performance before actual manufacturing, saving time and cost and enhancing the quality of results.

This study analyzes the photovoltaic performance of $MASnI_3$-based solar cells using the SCAPS-1D simulation tool, with the primary objective of optimizing their efficiency. The optimization process focuses on thickness adjustements and doping concentration variations. Various ETL materials were investigated to enhance solar cell performance. Finally, the effects of temperature variations and defect concentrations on device efficiency were systematically examined.

Thesis Structure :

- Chapter One

A general introduction to solar cells and their photovoltaic operation mechanism, with a review of the development of cell technology from the first generation to perovskite cells.

- Chapter Two

Focuses on the electrical properties of perovskite materials, analyzing their crystalline structure and technical features and perovskite solar cells.

- Chapter Three

Provides a detailed overview of the SCAPS program, its advantages in numerical modeling, and its mechanism for simulating multilayer solar cells.

- Chapter Four

Presents the simulation results obtained for $MASnI_3$ cells, and analysis the impact of various parameters on cell efficiency.

- Conclusion

Summarizes the main findings and the conclusions drawn from the research.

CHAPTER I:

GENERAL INFORMATION ON PHOTOVOLTAIC CELLS

Chapter I

General information on photovoltaic cells

1.1. Introduction

Today, photovoltaic is one of the renewable energy technologies that plays a major role in the future of global electricity production. In this chapter, we give an overview of solar and photovoltaic energy, including the solar cell, their characteristic parameters, as well as the advantages and disadvantages of photovoltaic cells.

1.2. Solar energy

Photovoltaic solar energy comes from the direct transformation of part of the light into electricity. This conversion is carried out by means of a so-called photovoltaic (PV) cell based on a physical phenomenon called the photovoltaic effect which consists of producing an electromotive force when the cell is exposed to light. The generated voltage can vary depending on the material used to manufacture the cell [1].

1.2.1. Solar radiation

The sun is a star. Her surface temperature is estimated at approximately 5800 K, the distance between the sun and the earth is approximately 149,597,890 km. The sun emits a huge quantity of radiant energy which is solar radiation. There are three types [2]:

- Direct radiation: it reaches the ground without losing energy.
- Diffuse radiation: it reaches the ground after having spread through the atmosphere and the clouds.
- Reflected radiation: this is the incident radiation reflected by the earth's surface.

Solar radiation is electromagnetic radiation that extends over an ultraviolet wavelength (0.2 μm), infrared (2.5 μm), visible (0.3 μm violet, 0.8 μm red). The atmosphere reaches approximately 1360W/m2 of this radiation. The distance crossed by solar radiation in the atmosphere is called air mass AM. It is a function of the angle of incidence θ relative to the zenith. It is worth [3];

AM= 1/ cos θ ……(I.1)

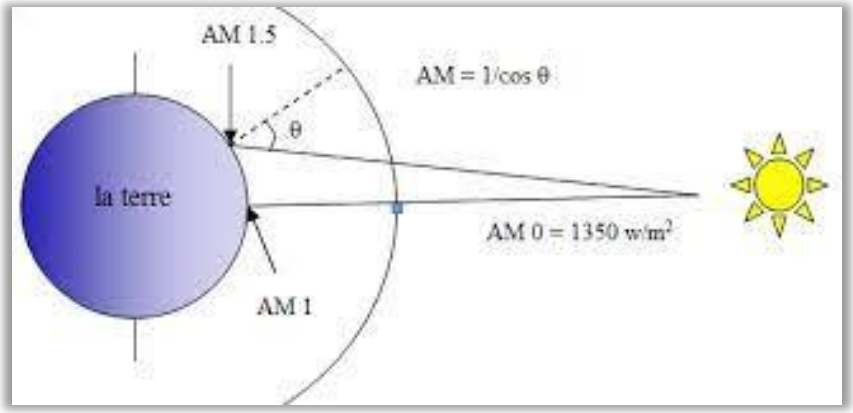

Figure I.1: Standards for measuring the spectrum of light energy emitted by the sun, Concept of the AM convention

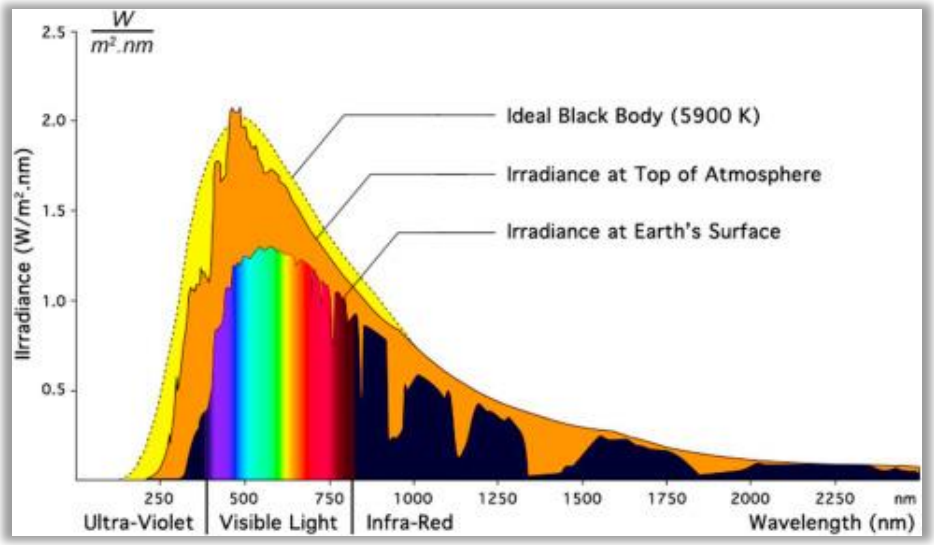

Figure I.2: Spectral distribution of solar radiation

The decomposition into wavelengths or (colors) is the spectrum of the sun. Sunlight is indeed composed of all kinds of colored radiations, characterized by their wavelength range. The photons, light grains that make up this electromagnetic radiation, carry an energy which is connected to the wavelength by the relation [4]:

$E = hv = \frac{hc}{\lambda}$ ……(I.2)

h: Planck constant,

λ: The wavelength.

c: speed of light.

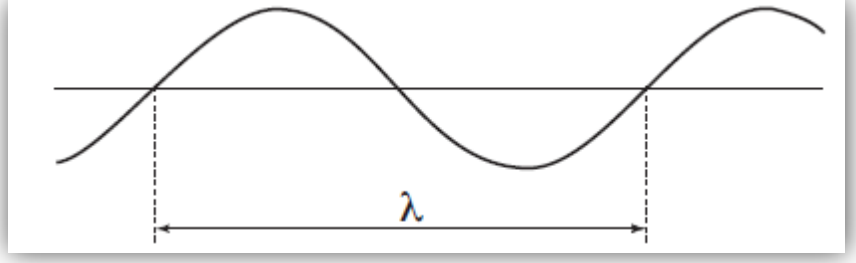

Figure I.3 : Wavelength definition (λ).

The energy associated with this solar radiation decomposes approximately to :

Table I.1 : The wavelength of the different radiations.

Radiation	Wavelength	Percentage
Ultraviolet UV	0.20< λ<0.38µm	6.4%
Visible	0.38< λ<0.78µm	48%
Infrared IR	0.78< λ<10µm	45.6%

The direct relationship between the energy of a photon is expressed in electronvolts and its wavelength in micrometers [5].

$$E(ev) = \frac{1.24}{\lambda(\mu m)} \quad \text{.....(I.3)}$$

1.3. Photovoltaic cell

1.3.1. Definition

Photovoltaic cells (The word "photovoltaics" (PV) is composed of two words; "photo" meaning light and "voltaic" (after the name of the Italian physicist Alessandro Volta (1745-1825) which is the first electrochemical battery) which means electricity) are semiconductor electronic components (usually made of silicon in its various forms). They directly convert the light energy into low-voltage direct current electricity (photovoltaic effect). Since the light energy is the sun, we call it solar cells [6].

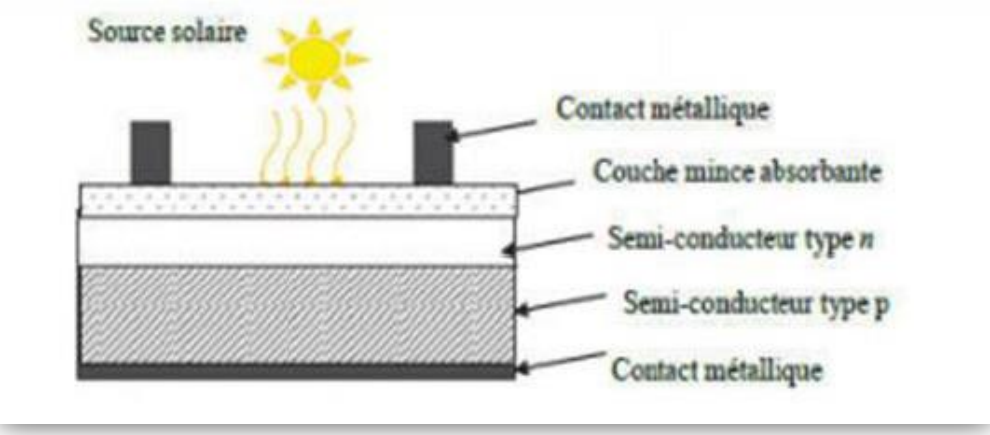

Figure I.4 : Representation of the structure of a single photovoltaic cell.

1.3.2. Photovoltaic effect

The photovoltaic effect is a phenomenon that allows the conversion of light energy into electricity, through a semiconductor material responsible for the transport of electrical charges as shown in Figure I.5 [7]:

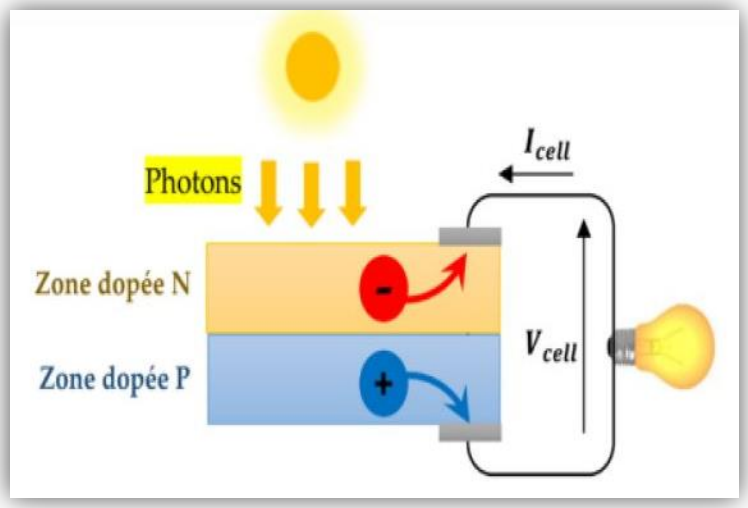

Figure I.5 : Schematic of the photoelectric conversion.

1.3.3. History of photovoltaic cell

The word photovoltaic comes from the Greek word "photos" which means light and voltaic of the Italian physicist "Alessandro volta" who invented the battery in 1800 and named it after the volt voltage measurement unit. The first to discover the photovoltaic effect was

the French physicist, Alexandre Edmond Becquerel, who observed the appearance of the voltage generated by sunlight in 1839 [8].

- 1839: French physicist Edmond Becquerel discovers the photovoltaic effect.
- 1875: Werner Von Siemens publishes an article on the photovoltaic effect in semiconductors before the Berlin Academy of Sciences. But until the Second World War, this was still an anecdotal finding.
- 1954: Three US researchers, Chapin, Pearson and Prince, develop a high-efficiency photovoltaic cell as the emerging aerospace industry seeks new solutions to power its satellites.
- 1958: Development of a battery with an efficiency of 9%. The first solar-cell-powered satellites have been launched into space.
- 1973: The first house powered by photovoltaic cells is built at the University of Delaware.
- 1983: The first Australian car using photovoltaic energy travelled 4,000 kilometres.
- 1995: Start of grid-connected photovoltaic roof plan, Japan and Germany are popularised since 2001[9] [10].

1.3.4. Principle of operation of a solar cell

The photovoltaic cell is an electronic device intended to generate electrical energy if it receives solar energy in the form of radiation. Its structure is a PN junction composed of two layers: a P-type layer and an N-type layer. When the P-layer is contacted with the N-layer, the excess electrons in the N-material diffuse into the P-material and the excess holes in the P-region diffuse into the N-region. The initially doped N-area becomes charged positively, and the initially doped P-area negatively charged. An electric field is created between them that tends to push the electrons in the n zone and the holes towards the p zone. By adding metal contacts on the n and p zones, a junction (called p-n) is obtained.

When the photons from the sun hit the cell, some are reflected and others are transmitted or absorbed into the solar cell, only the absorbed photons participate in the photoelectric effect. The absorbed photons of energy equal to or greater than the width of the forbidden band communicate their energy to the atoms, each one passes an electron from the valence band into the conduction band and also leaves a hole able to move, Thus generating an electron-hole pair.

In the space charge zone, the electron-hole photo-generated pairs will be drawn by the electric field to the N region (electrons) and the P region (holes). This displacement of the photo-carriers gives birth to a photo-current of generation. Photovoltaic conversion involves three physical phenomena, closely related and simultaneous:

- The absorption of light in the material.
- The energy transfer from photons to electrical charges.
- Collection of charges.

The first phenomenon is the optical absorption of photons by a suitable semiconductor material in the most intense part of the solar spectrum. The optimum value of the gap of the material used as absorber is usually around 1.5 eV. The second phenomenon concerns the rapid separation of electrons and holes before their recombination. The third relates to the drive of electrons and holes towards collecting electrodes (carrier collection).[11]

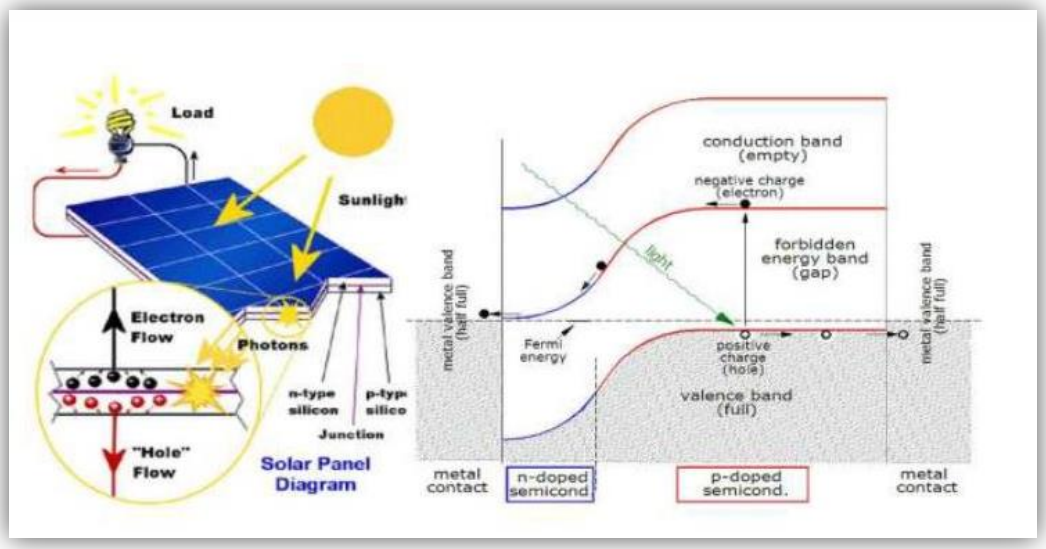

Figure I.*6*: Principle of operation of a photovoltaic cell.

1.4. Characteristic of a photovoltaic solar cell

The resulting photocurrent is the sum of three components, the scattering current of the photoelectrons in the P-type region, the photo-generating current in the space charge zone and the scattering current of the photo-electronsholes of the N-type region. These different contributions are added to create a resulting photocurrent I_{ph}, which is a minority carrier

current proportional to the light intensity. This current is in opposition to the diode current, called the dark current I_{obsc}, which results from the component's polarization.

The current delivered to a charge by an illuminated photovoltaic cell is written :

$$I(V) = I_{ph} - I_{obsc}(V) \quad \text{.....(I.4)}$$

With

$$I_{obsc}(V) = I_s \left[\exp\left(\frac{qV}{nkT}\right) - 1\right] \quad \text{.....(I.5)}$$

V : Voltage at the junction terminals (Volt)

I_s is the saturation current of the diode used as a reminder that a solar cell in the dark is simply a semiconductor rectifier, or diode.

n is the diode's ideal factor (equal to 1 if the diode is ideal and equal to 2 if the diode is entirely governed by generation/recombination) [12].

Current I is usually related to a surface: the current density J is expressed in $mA.cm^{-2}$.

1.4.1. Current – voltage Characteristic (I-V)

The photovoltaic cell is nothing more than a photodiode that works without external polarization and takes its photo current into a charge. Under illumination the I(V) characteristic of the diode no longer passes through the origin of the coordinates, there is a region in which the product I*V is negative (figure I.7), the diode provides energy [13].

The plot of the I-V characteristic is shown in figure (I.7) which shows the variation of the current as a function of the voltage for a typical solar cell.

In darkness, the curve is identical to that of a single diode, but under illumination, the curve is offset downwards with a value I_{ph} (photo-current).

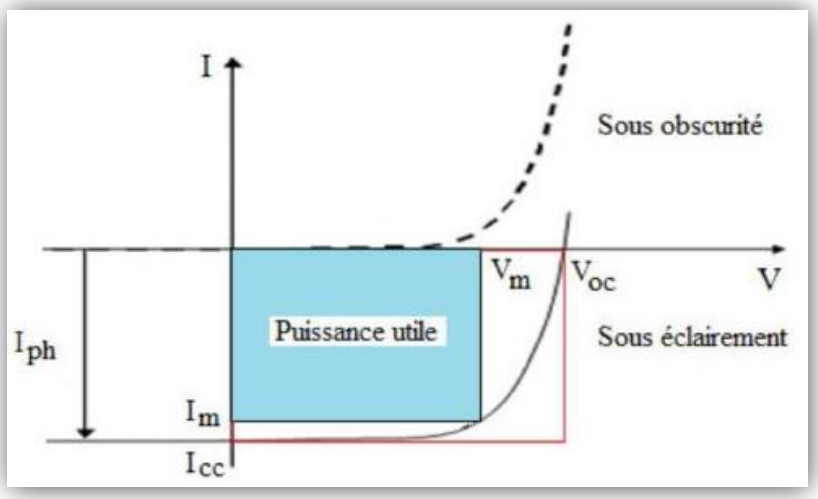

Figure I.7: Current-voltage characteristic of a solar cell.

1.4.2. Electrical parameters of a photovoltaic cell

The parameters of a photovoltaic cell can be determined from the current-voltage curves, or from the characteristic equation. These parameters allow you to compare different cells lit under identical conditions. The most common are:

- ✓ Short-circuit current Icc.
- ✓ Open circuit voltage Vco.
- ✓ Form factor FF
- ✓ Efficiency ŋ.
- ✓ Quantum efficiency (QE)

1.4.2.1. Short circuit current (Icc)

The short-circuit current expressed in mA, is the current that circulates in the cell under illumination and by shorting the terminals of the cell. It grows linearly with the intensity of the cell illumination and depends on the illuminated surface, the wavelength of the radiation, the mobility of the charge carriers and the temperature [14]. In the ideal case (Rs zero and Rsh infinite), this current is confused with the current photo I_{ph} otherwise, canceling the voltage V in equation (I.6) [14].

$$I_{cc} = I_{ph}/[1 + \frac{Rs}{Rsh}] \quad \text{.....(I.6)}$$

1.4.2.2. Open circuit voltage (Voc)

Open circuit voltage is defined as the maximum voltage generated by the photovoltaic cell. It represents the voltage at the terminals of the cell under illumination without charge circuit, that is to say when the current passing through the cell is zero. It depends on the energy barrier and the active layer material.

The voltage V is given by the relation:

$$V_{co} = \frac{KT}{q}\left(Ln\ \frac{I_{cc}}{I_s} - 1\right) \quad \text{(I.7)}$$

K : Boltzmann's constant

T : the absolute body temperature.

q : I_{ph} electron charge: photocurrent

I_s : diode saturation current

1.4.2.3. Form factor (FF)

The form factor FF is an important parameter to define the quality of a cell. This is the ratio of the maximum power delivered by the cell P_{max} to the product of the short-circuit current Icc by the open-circuit voltage Vco (that is, the maximum power of an ideal cell). The form factor indicates the quality of the cell the closer it is to the unit the more the cell is performing, it is around 0.7 for performing cells; it decreases with temperature. It reflects the influence of losses by both parasitic resistances Rs and Rsh [14]

It is expressed as follows:

$$FF = \frac{P_{max}}{I_{cc}*V_{co}} = \frac{I_{max}*V_{max}}{I_{cc}*V_{co}} \quad \text{(I.8)}$$

where Imax and Vmax represent the current-voltage density torque for which the power delivered by the cell is maximum (P_{max}). The theoretical FF form factor is between 0.25 and 1.

1.4.2.4. Efficiency (η)

This is the most important parameter of a cell because it allows to evaluate these performances. It is defined as the ratio between the maximum power delivered by the Pm cell and the light output Pin of the light radiation.

$$\eta = \frac{Pm}{Pin} = \frac{FF*V_{oc}*I_{cc}}{Pin} \quad \text{.....(I.9)}$$

1.4.2.5. Quantum efficiency (QE)

Quantum efficiency describes the probability, for an incident photon of a given wavelength, to create an electron-hole pair actually collected by the cell. It is expressed in the following equation:

$$QE(\lambda) = \frac{I_{ph}}{q\phi_0(\lambda)} \quad \text{.....(I.10)}$$

Where I_{ph} is the photocurrent at wavelength λ, q is the charge of an electron, $\phi_0(\lambda)$ is the flux of photons incident at wavelength λ.

Two types of quantum efficiency are often considered in the case of solar cells:

- The external quantum efficiency (EQE), which takes into account optical loss effects such as unabsorbed light or reflected light.
- Internal quantum efficiency (IQE), it does not take into account the transmitted photons (incomplete absorption) and reflected.

Internal quantum efficiency and external quantum efficiency are linked by the following relationship:

$$IQE(\lambda) = \frac{EQE(\lambda)}{1-R(\lambda)} \quad \text{.....(I.11)}$$

Where R(λ) is the reflection coefficient.

The quantum efficiency, obtained as a function of the wavelength of the photons (λ), corresponds to the number of electrons collected relative to the number of incident photons having a given wavelength. By calling this curve with the illumination spectrum, we can determine the current generated in the cell. In addition, this curve is a good tool to try to identify the layers or interfaces of the solar cell that cause absorption losses. Quantum efficiency depends primarily on the absorption coefficient of the materials used, the ionisation potential, and the collection efficiency [15].

1.5. Equivalent electrical diagram

1.5.1. Ideal cell

In the ideal case, the cell of a PN junction subjected to photovoltaic illumination connected to a load can be schematically represented by a current generator I_{ph} in parallel with a diode delivering a current. The following Figure shows the equivalent circuit of an ideal solar cell.[16]

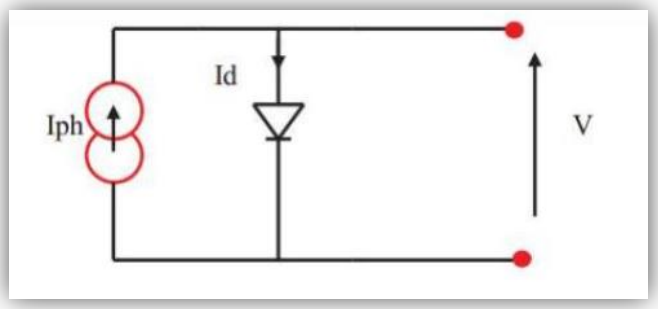

Figure I.8 : Electrical diagram of an ideal solar cell.

Under the dark, the current in such a p-n junction type structure is called the dark current and has the following form [17] :

$$I_{obs} = I_s[\exp\left(\frac{qV}{nkT}\right) - 1] \quad \text{.....(I.12)}$$

With:

q : elementary charge q =1.6. 10 (-19) C

V : Junction voltage (V)

k : Boltzmann constant =1.38.10-23 J.K-1

T : temperature (K)

I_s : inverse saturation current of p-n junction

n: ideal coefficient of the junction

This dark current corresponds to the diode current (I_{obs}), it results from the polarization of the junction.

Under illumination, a term I_{ph}, taking into account the generated photo-current is added. The equivalent electrical circuit of an ideal solar cell under illumination is obtained, which is represented by the following equation:

$$I = I_{ph} - I_{obs} = I_{ph} - I_s[\exp\left(\frac{qV}{nkT}\right) - 1] \quad \text{.....(I.13)}$$

1.5.2. Real cell

The performance of a solar cell is limited by the influence of two physical phenomena comparable to two resistances Rs and Rsh (figure I.9).[18]

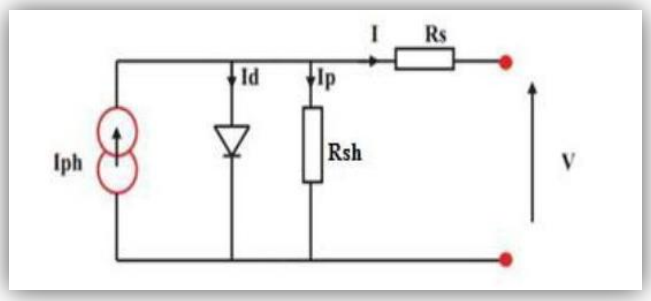

Figure I.9 : Electrical diagram of a real solar cell.

Rs : Series resistance, mainly due to losses by Joule effects through the collection grids and the own resistance of semiconductors, as well as bad contacts (Semiconductor, electrodes).

Rsh : Parallel resistance, called «Shunt», comes from losses by recombination due mainly to the thickness, surface effects, as well as the non-ideality of the PN junction.

The output current of a photovoltaic cell is calculated in the following mathematical form:

$$I = I_{ph} - I_s\left[\exp\left(\frac{qV}{nkT}\right) - 1\right] - \frac{V+R_sI}{R_{sh}} \quad \text{.....(I.14)}$$

Where:

I_{ph} : Photonic Current of the diode (A).

I_s : Reverse saturation current of the diode (A).

q : Electron charge (1.603×10^{-19} C)

n : The diode's technology-dependent (material) ideal factor is generally between 1 and 2.

k : Boltzmann constant (1.38×10^{-23})

1.6. Photovoltaic sectors

Today, a wide variety of photovoltaic cells exist and can be divided into three main families according to the technologies used.

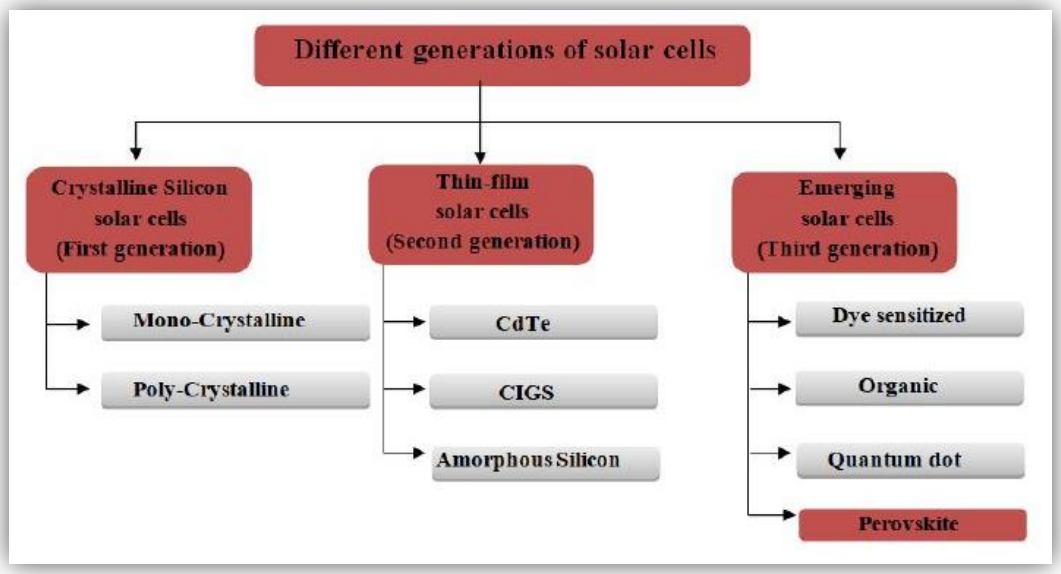

Figure I.10 : Solar cells three generations with photovoltaic materials.

1.6.1. First generation: solar cells is silicon based

a) Monocrystalline silicon

PV panels with monocrystalline cells are the first generation photopiles, they are made from a block of silicon crystallized into a single crystal. If single-crystal cells have a yield of 12 to 18%, they can produce a lot of energy on a small space (about 150 Wc/m²) and have a life span of 25 years. However, these cells are not working with strong sunlight and have a costly and laborious production method. [18]

Figure I.11: Silicon monocrystalline cell.

b) Polycrystalline silicon

PV panels with poly crystalline cells are made from a block of crystallized silicon in the form of multiple crystals. These cells produce a power of about 100 Wc/m², and they have an efficiency of 11 to 15% and an estimated life of 30 years. Today, cells based on poly crystalline Si have been established thanks to their potential for increasing productivity. The advantage of these cells is their low production cost and their ratio of manufacturing energy 2 to 3 times lower compared to silicon-based monocrystalline cells. [18]

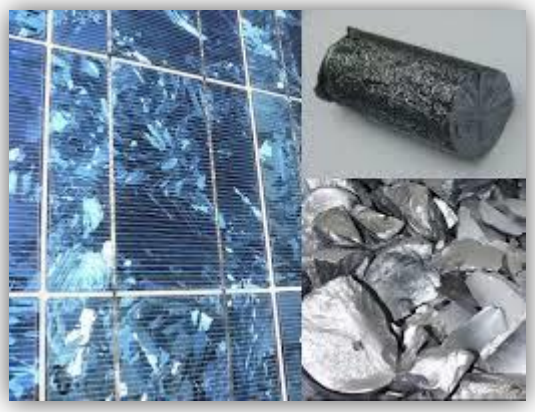

Figure I.12: Polycrystalline cell.

1.6.2. Second generation solar cells

a) Amorphous silicon

Silicon gas is evaporated on a support of soft glass, plastic or metal. These cells appeared in 1976, it is dark gray color. Amorphous silicon cells, its atoms are turbulent, so it absorbs more light than monocrystalline cells. They are used in small machines such as calculators and watches. This type of silicon is less expensive to manufacture and cost-effective.Its efficiency is low between 8% and 10.7%.

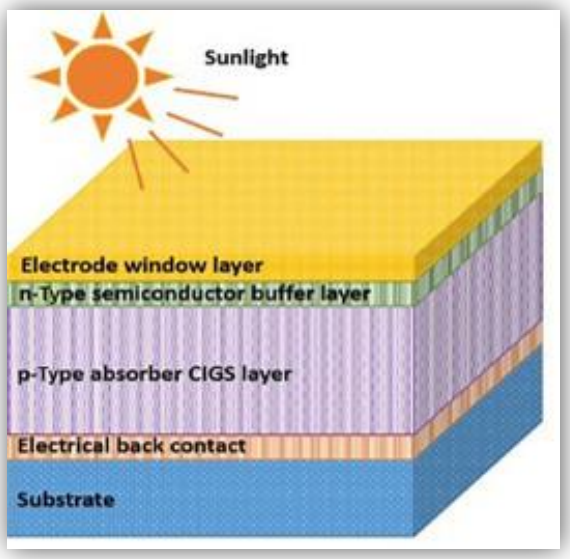

Figure I.13: Amorphous silicon cell.

b) Copper and indium selenide (CIS or CIGS)

CIGS is a semiconductor. It needs an N-type material to create a p-n junction. The CIGS cells of type heterojunction, it contains an absorbent made of copper, gallium, indium and selenium, it was realized in 1975 by "S.wagner et coll de Bell Télephone". The advantage of these cells is their yield of 23.4% in 2019, but it takes a lot of space to achieve good production.[19]

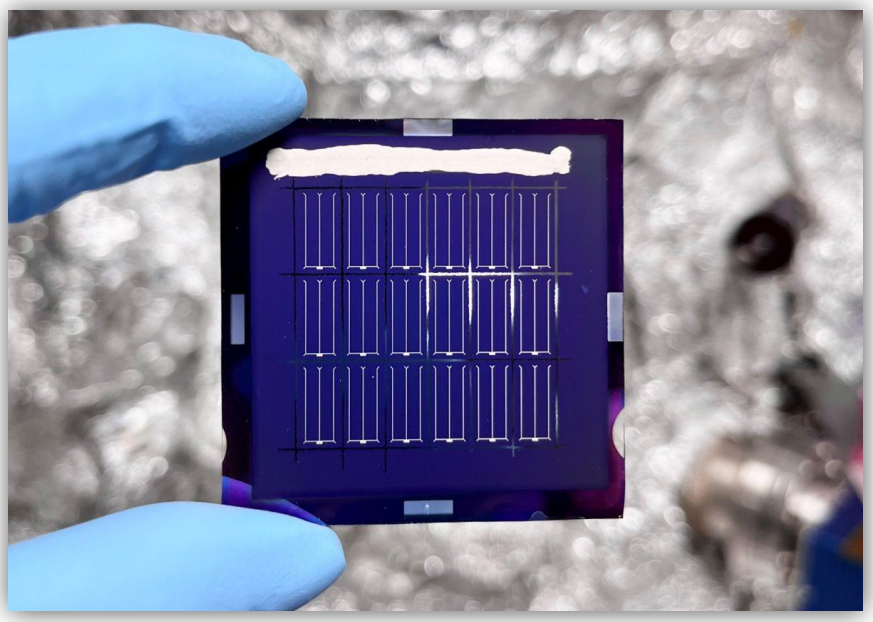

Figure I.14 : CIGS solar cell.

c) Cadmium telluride (CdTe)

Cadmium tellurium is a P-type semiconductor that requires another N-type material (CdS,SnO2....) to create a p-n junction. It was studied in 1960 and developed in 1972.

The CdS/CdTe solar cells are produced by evaporating a thin layer of CdS over a layer of conductive glass followed by another evaporation of a thick layer of CdTe. The cell is then treated for a short period of time at 450 °C. These cells have a high efficiency of 22.1% in 2015 [24] and their absorption coefficient is high.[20]

Figure I.15 : CdTe solar cell.

1.6.3. Third generation solar cells

a) Organic cells

The photovoltaic effect has been observed in organic materials for more than 40 years, since this sector has experienced the best growth rate among the different photovoltaic sectors during the last 12 years. The latest developments in this field have led to yields of 13.2%. Its large-scale development is now being hampered by the low mobility of the carriers in the material, limiting the yield, and the short life span of the cells. Despite these advantages, there are disadvantages such as its short life span [19].

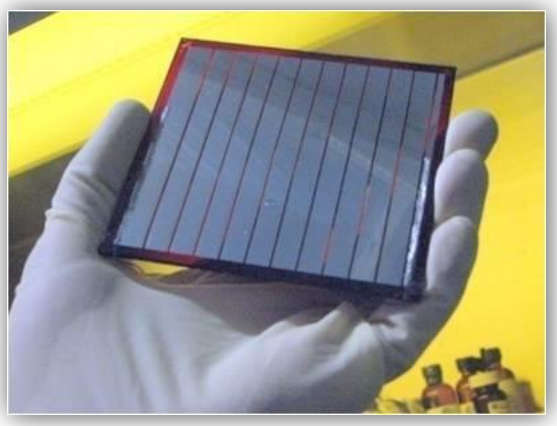

Figure I.16: Organic solar cell.

b) Perovskite cell

This element is most often embodied in an organic-inorganic hybrid of lead or a tin halide (in its active layer). From a share of 3.8% in 2009 to 22.1% in 2016 [The advent of hybrid perovskite has amazed photovoltaic research groups as it has demonstrated high performance and rapid growth over the last 5 years. These materials have resulted in an increase in the energy conversion efficiency (ECP) for photovoltaic (PV) devices of over 20% . The following figure represents a solar cell of Perovskite.[21]

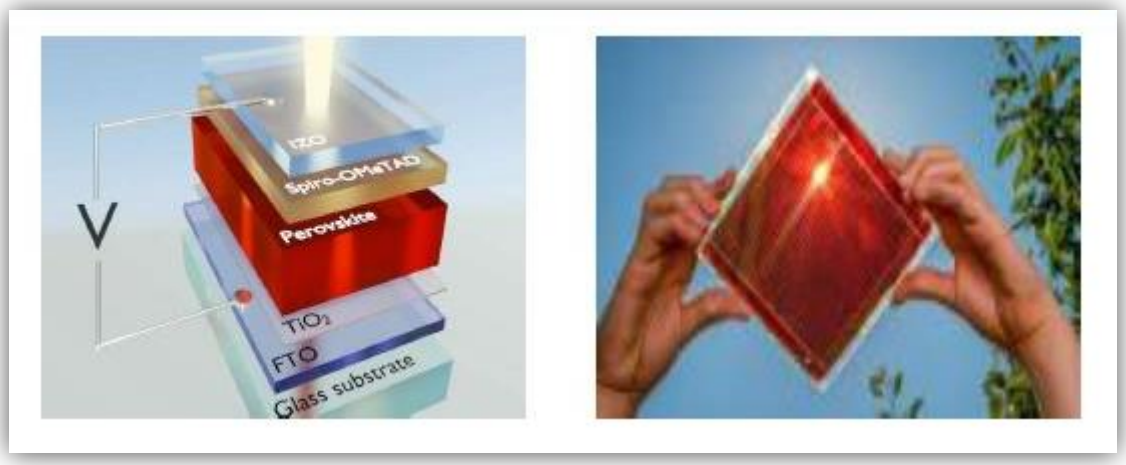

Figure I.17: Perovskite solar cell.

1.7. Advantages and disadvantages of photovoltaic cells

1.7.1. Advantages

The following are the benefits that make photovoltaic cells an efficient renewable energy source:

- The conversion of electricity from sunlight or solar radiation is direct. This eliminates the need to install a cumbersome generator.
- Solar power generation is environmentally friendly. A photovoltaic panel provides clean and green energy. There is no gas emission during electricity generation.
- Free of fuel and water.
- Solar energy is generated by nature, it's free and simple.
- Where sunlight is available, solar energy can be easily generated. • Photovoltaic energy is suitable for smart power grids with distributed electricity generation.
- Photovoltaic cells do not have a mechanically movable part like in wind turbines, so they have less breakage and also require little maintenance than other renewable energy sources.
- The photovoltaic panels are completely silent and do not produce any noise. • They can be used in remote areas where the installation of an electrical network is too expensive.
- Photovoltaic panels are easily installed on the ground or roofs of residents without interference from residential lifestyle.
- They have a long life span of up to 30 years [21].

1.7.2. Disadvantages

- The manufacture of photovoltaic panels is high-tech, requires a lot of research and development, and therefore requires expensive investments.
- For home installation, a backup system (battery) is required.
- The investment cost of photovoltaic installations is very high.
- Batteries are needed to store energy which affects cost and performance.
- Cell yield is low at 40%.
- A life cycle in question: the life of a photovoltaic installation is not eternal but in the range of 20 to 30 years.

1.8. Photovoltaics in Algeria

Recently, solar energy has proved to be one of the alternative solutions for our dependence on fossil fuels, this clean, inexhaustible energy provides ten thousand times

more energy than that consumed by the entire world population (Funk, 2010). As a result, developing this sector remains a priority for many countries in order to achieve sustainable development on these three dimensions: economic, social and environmental [22].

Algeria is starting a green energy dynamic by launching an ambitious renewable energy (RES) and energy efficiency development program. This vision of the Algerian government is based on a strategy focused on developing inexhaustible resources such as solar energy and using them to diversify energy sources and prepare for the future of Algeria. Through the combination of initiatives and intelligence, Algeria is embarking on a new era of sustainable energy.

The updated renewable energy programme is to install 22,000 MW of renewable power by 2030 for the domestic market, with export as a strategic objective. if market conditions permit.

The updated energy efficiency programme aims to achieve energy savings of around 63 million TOE by 2030, for all sectors (building and public lighting, transport, industry) by introducing high-performance lighting, Thermal insulation and solar water heaters, clean fuels (GPLc and GNc), and high-performance industrial equipment.

The energy efficiency program will reduce fossil fuel CO2 emissions by 193 million tonnes.

The main projects implemented and currently in progress in the field of renewable energies are as follows:

- ✓ Construction of the first 150 MW hybrid solar/gas power plant in Hassi R'mel.
- ✓ Construction of the first 10 MW wind farm.
- ✓ Solar power programme in 20 villages in the South:
- ✓ Installation of about 1 million km² of photovoltaic area.
- ✓ Production to date of 2 GWh.
- ✓ Construction of a plant for the manufacture of photovoltaic modules and installation of solar panels Industrial Zone of Rouiba with a capacity: 41 800 photovoltaic module/year [23].

1.9. Conclusion

In this chapter we have conducted an abridged bibliographical study on photovoltaic solar cells, their general operating principle, describing their parameters and characteristics. The different photovoltaic sectors have also been identified.

CHAPTER II:

THE PEROVSKITE SOLAR CELLS

Chapter II

The Perovskite Solar Cells

2.1. Introduction

In order to develop cost-effective alternative photovoltaic systems to silicon solar cells, perovskite solar cells have attracted considerable interest in recent years. Today, the efficiency of these solar cells has reached high levels, surpassing the efficiencies of many commercial photovoltaic cells.

This chapter is the subject of a study on solar cells perovskites, we start with general about perovskites, then the principles of operation of the solar cell perovskite, as well as defects in the structure perovskite. Finally, the advantages of hybrid perovskites.

2.2. General about the perovskites

2.2.1. History

The origin of "perovskite" dates back to the 1830s, when Gustav Rose (Gustav Rose) first discovered calcium titanate (CaTiO3) and standardized it in honor of the Russian mineralogist L.A. Perovski .

Since then, the definition of perovskite has been extended to include compounds with a crystal structure similar to CaTiO3 [24].

Among these compounds, a family of organic-inorganic hybrid perovskites appears which mainly comprises two subfamilies: 2D perovskite and 3D perovskite [25].

Since the 1990s, the two-dimensional hybrid perovskite crystal has attracted the interest of researchers because of its very interesting emission characteristics, and has become a promising candidate for the realization of various optoelectronic devices (such as Organic Light Emitting Diodes (OLEDs) and Organic Field Effect Transistors (OFETs)) [2]. In recent years, the mobility of each layer carrier in OFETs has increased sharply from 10 4 to 1 cm2/V-s (compared to amorphous silicon cells) [26].

Since 2012, 3D hybrid perovskites, particularly compounds with the chemical formula CH3NH3PbI3, have become very promising absorbers for solar cells and have shown outstanding performance in a short time .

Therefore, hybrid perovskite halides cells were introduced into the NREL (National Renewable Energy Laboratory) solar cell efficiency charter as an emerging photovoltaic industry: The number of people in the labour market is growing rapidly. The last point shows that the best recent certification efficiency is 22.1% [2]. This impressive short-lived development is unprecedented and revolutionising solar cell research [25].

2.2.2. Crystalline structure of the Perovskites

The crystalline structure of perovskite with a general chemical formula ABX3 can accommodate a multitude of different elemental combinations, it is the most abundant class of minerals on Earth. The structure is shown in Figure II.1, cation A occupies the eight vertices of a cube surrounded by twelve X anions, while cation B is at the center of an octahedron formed by six X anions [BX6]4- located at the centers of the cube faces [27].

It is broken down into two groups: inorganic perovskites, which are in the form of oxides, and halogenated perovskites, which can be inorganic or hybrid (organic-inorganic). Table II.1 shows the different compounds for each perovskite [28].

Table II.1 : The different molecules corresponding to the different families of perovskite.

	Oxide	**Inorganic halogenated**	**Hybid halogenated**
A	Divalent cation ($Mg^{2+}, Ca^{2+}, Sr^{2+}, Ba^{2+}$….)	Monovalent alkali metal (Li^{+}, Na^{+}, K^{+}, ….)	Small organic molecule (MA (methylammonium), FA (formamidinium)…)
B	Metal cation ($Ti^{4+}, Si^{4+}, Sn^{4+}$, ….)	Divalent ionic metal (Pb^{2+}ou Sn^{2+})	
X	Oxygen	Halogen (Cl^{-}, Br^{-}ou I^{-})	

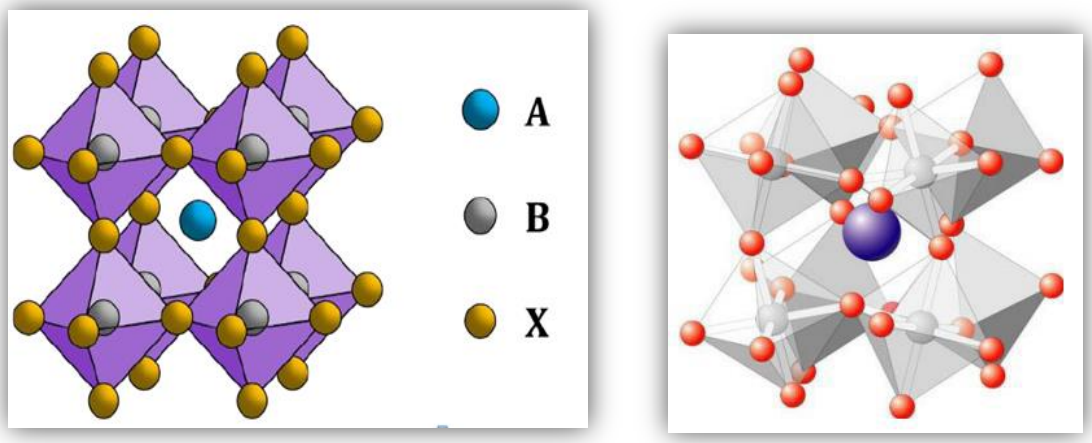

Figure II.1 : Perovskite structure.

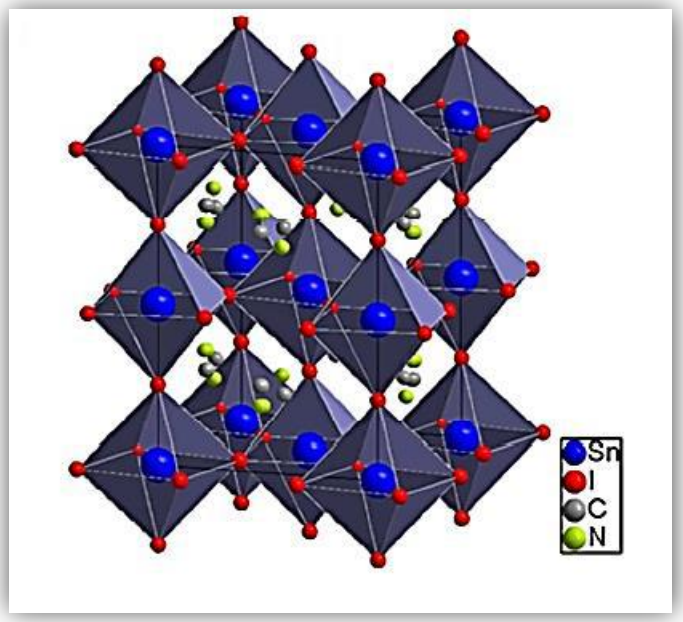

FigureII.2: Crystalline structure of CH3NH3SnI3 showing the tetragonal structure of the perovskite lattice

2.3. Solar cells based on perovskite materials

A perovskite solar cell consists of a glass/FTO substrate on which the fluorine-doped tin oxide FTO is deposited, and on FTO titanium dioxide TiO2 is deposited. TiO2 is used to improve electron transport. The active layer consists of a perovskite material. To improve the transport of holes, a layer of spiro-OMeTAD is deposited between the electrode in Gold. The resulting structure is shown in Figure II.3 (a). The topography of a glass-type

perovskite/FTO/TiO2/Perovskite/Spiro-OMeTAD/Au cell with the SEM scanning electron microscope is shown in Figure II.3(b) [29].

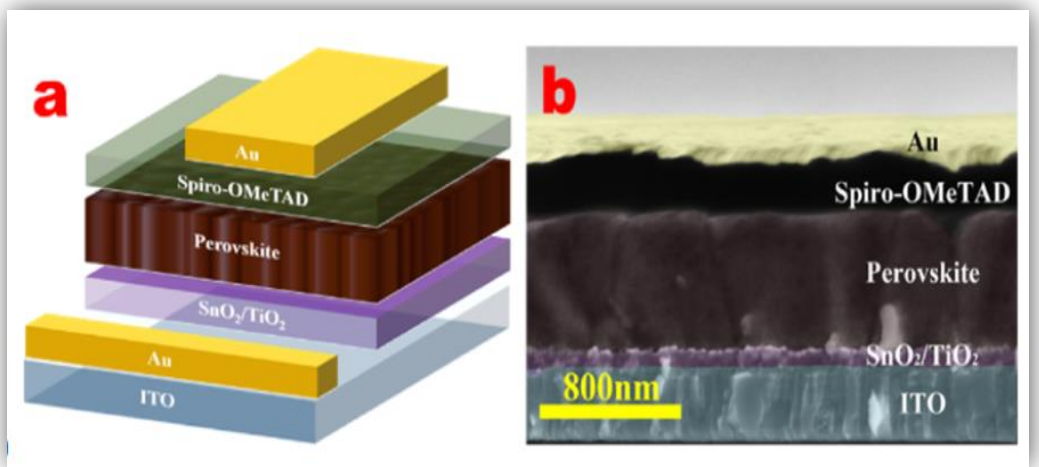

Figure. II.3 : (a) Structure diagram of PSC units. (b) Cross-view scanning electron microscope (SEM) images of PSC units

2.4. Perovskite layer manufacturing techniques

The main techniques for the deposition of perovskite films are vacuum deposition (single-step precursor deposition, sequential vapour deposition, double-source vacuum deposition) and solution processing (one-step spin-coating, two-step spin-coating, spray and CBD) where the most frequently applied method is spin-coating. Figure II.8 lists the general methods for the preparation of perovskite films. Perovskite films must have: total coverage of the ETL or BL surface, small roughness and grain size up to micron scale. The perovskite layers have many advantages: a large capacity of absorption of light, appropriate energy levels for the proper transfer of load carriers within the cell, a structure that minimizes recombination phenomena and good value for money. Unfortunately, perovskite layers are very sensitive to moisture, their composition is not consistent with the original environmental approach and long-term stability remains a major challenge [30].

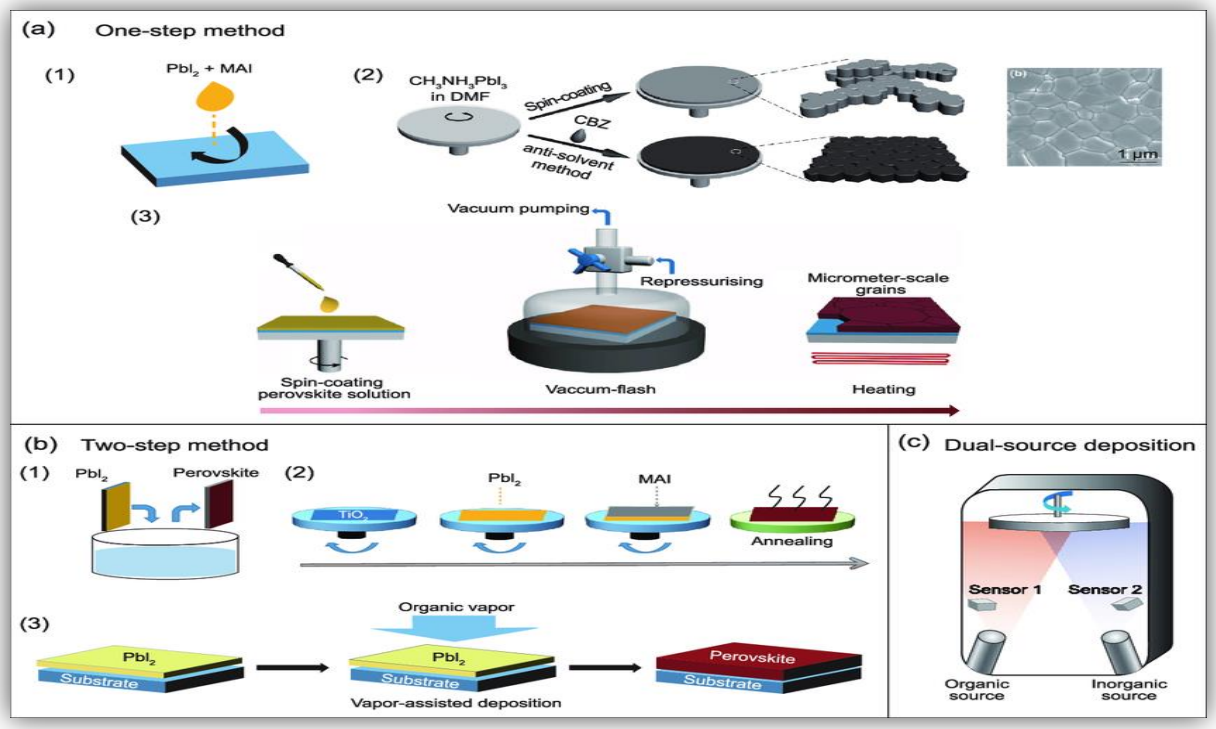

Figure II.4: Three general perovskite film fabrication methods

(a) one-step precursor deposition method (CBZ: chlorobenzene); (b) sequential deposition method; (c) dual-source vapor deposition method.

2.5. Opto-electronic properties

The interest in perovskite ABX3 for more than four decades results in the ease of changing the nature of cations A and B present in the structure. This modification of the elements causes a change in the properties of the material, thus leaving open the door to all kinds of physical properties depending on the chemical and electronic nature of the two atoms A and B [31].

2.5.1. Optical properties

Hybrid perovskites are characterized by their direct energy gap (DG) and high light absorption coefficient, making them highly effective in photovoltaic applications. For example, the absorption coefficient of the iodine perovskite $MAPbI_3$ is estimated to be 1.5×10^5 cm^{-1} at a wavelength of 550 nm, a value close to that of conventional photovoltaic materials such as GaAs, CdTe, and CIGS.

The absorption coefficient of these materials generally ranges between 10^4 and 10^5 cm^{-1}.

$MAPbI_3$ perovskites have an energy gap (GAP) of 1.50 to 1.55 eV, making them well-suited for solar energy applications.

The value of this gap varies depending on the composition of the material. The smaller the electronegativity difference between the cation and anion in the chemical structure, the lower the gap. For example, replacing part of the iodine with bromine increases the conduction band (BC) energy and decreases the valence band (BV), altering the absorption properties.

The bandgap for the $CH_3NH_3PbBr_3$ structure is estimated at approximately 2.2 eV.

Also, when the ratio of iodine to chlorine (x in the $CH_3NH_3PbI_{3-x}Cl_x$ structure is adjusted, the resulting mixture exhibits good light absorption and increased photovoltaic efficiency, which is reflected in the performance of the solar cell.

Due to the toxicity of lead (Pb), research has been conducted to find alternatives for it in the perovskite composition. One of the most prominent candidates is Sn (tin) in the formula $CH_3NH_3SnI_3$ (MASnI3).

Although it has attracted considerable attention, its resulting energy gap is still very low, and the material is unstable in air. Cells made with it reached an efficiency of about 6%, according to a study published in 2014 by Snaith's team, but there has been little progress since then.

Researchers from the University of Queensland have set a world record in solar cell efficiency using environmentally friendly perovskite technology.

A team led by Professor Lianzhou Wang unveiled a solar cell made from tin halide perovskite (THP), capable of converting sunlight into electricity with a certified record efficiency of 16.65% [32].

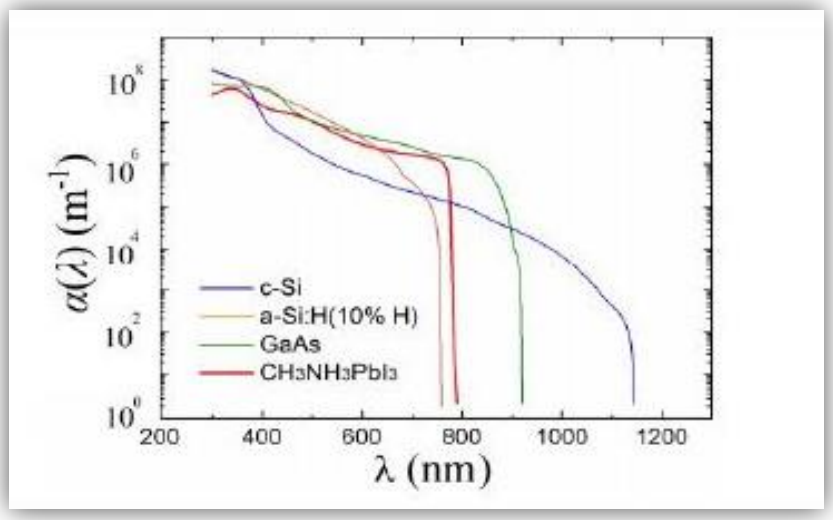

Figure II.5 : Material absorption curve: (λ) of c-Si, a-Si: H (10%H), GaAs and CH3NH3PbI3.

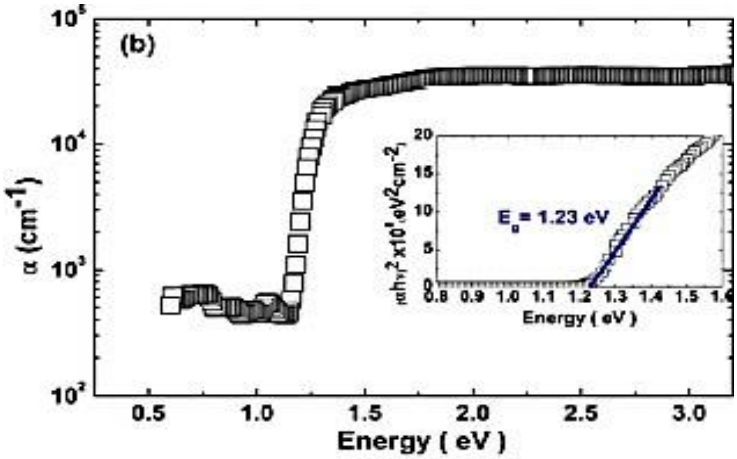

Figure II.6: The absorption profile of the material CH3NH3SnI3.

2.5.2. Electrical properties

The electrical properties are very interesting for photovoltaic application and are superconducting at relatively high temperatures, they transform mechanical pressure or heat into electricity (piezoelectricity), accelerate chemical reactions (catalysts) and suddenly change their electrical resistance when placed in a magnetic field (magnetoresistance), many electrochemical studies on electrodes based on these oxides have been carried out in aqueous media. They have revealed an important electro catalytic role in the oxygen electrode reaction at room temperature.

The perovskite becomes ionic and covalent, dual nature in electronic structures.

Experimental research shows the different values of band-ban for perovskites. The barring band of perovskite depends on the synthesis process and size of the organic/inorganic cation, metal ions and very less halogen ion [33].

2.6. Applications of perovskite

Perovskite plays an important role in industrial technology. They are used in solar cells and, based solely on their ferroelectric, dielectric, pyroelectric or piezoelectric properties, perovskite compounds have been incorporated into many applications [34].

2.7. Structure and Functioning of a Perovskite Solar Cell

The perovskite solar cell is a modern and promising technology in the field of solar energy conversion, known for its layered structure that enables high efficiency and ease of fabrication compared to traditional silicon-based cells. This type of solar cell typically consists of five main functional layers that work together to generate electricity. At the top of the structure lies the transparent conductive electrode, commonly made of indium tin oxide (ITO) or fluorine-doped tin oxide (FTO), which allows sunlight to pass through while maintaining good electrical conductivity. Directly beneath this is the electron transport layer (ETL), usually composed of titanium dioxide (TiO_2) or tin oxide (SnO_2), which is responsible for transporting the photo-generated electrons from the perovskite layer toward the negative electrode.

The core of the device is the active perovskite layer, which absorbs sunlight and creates electron-hole pairs. Two common types of perovskite materials are used here. The first is **$CH_3NH_3SnI_3$**, a lead-free perovskite that uses tin (Sn) as the central metal, offering an environmentally friendly alternative but with relatively lower stability. The second, more widely used type is **$CH_3NH_3PbI_3$**, which contains lead (Pb) and is known for its high power conversion efficiency and good stability, although it poses environmental concerns due to lead toxicity. Beneath the active layer lies the hole transport layer (HTL), made from materials such as Spiro-OMeTAD or PEDOT:PSS, which facilitates the movement of holes to the positive electrode and prevents recombination with electrons. Finally, the structure is completed with the back electrode, usually made of gold, silver, or carbon, which collects the

charges and closes the electrical circuit. In many designs, an encapsulation layer is added to protect the cell from environmental factors like moisture and oxygen, extending its operational lifespan. Thanks to this integrated and efficient design, perovskite solar cells are considered a highly promising solution for the future of renewable energy

Planar perovskite solar cells are categorized into two main types: the regular planar design (n-i-p) and the inverted planar design (p-i-n), with the difference lying in the sequence of layers and the direction of charge transport. In the regular n-i-p configuration, the cell typically starts with a transparent conductive glass substrate such as FTO, followed by an electron transport layer (ETL), usually made of TiO_2, then the perovskite active layer, a hole transport layer (HTL) such as Spiro-OMeTAD or PTAA, and finally a back metal electrode like gold or silver. In this setup, electrons move forward through the ETL, while holes travel backward through the HTL. Conversely, the inverted p-i-n structure begins with a hole transport layer (HTL), such as PEDOT:PSS or NiO, deposited on a transparent electrode like ITO, followed by the perovskite layer, an electron transport layer (ETL) such as PCBM or ZnO, and ends with the back electrode. In this arrangement, holes are collected at the front and electrons at the back. Each configuration has its advantages; the n-i-p design is more stable and widely used in laboratories, while the p-i-n design is easier to fabricate and better suited for industrial-scale printing. However, when using tin-based perovskites like $MASnI_3$, planar designs often face efficiency limitations due to the oxidation sensitivity of tin and the short charge carrier diffusion lengths. Despite this, ongoing research aims to overcome these challenges and improve the performance of planar tin perovskite solar cells.

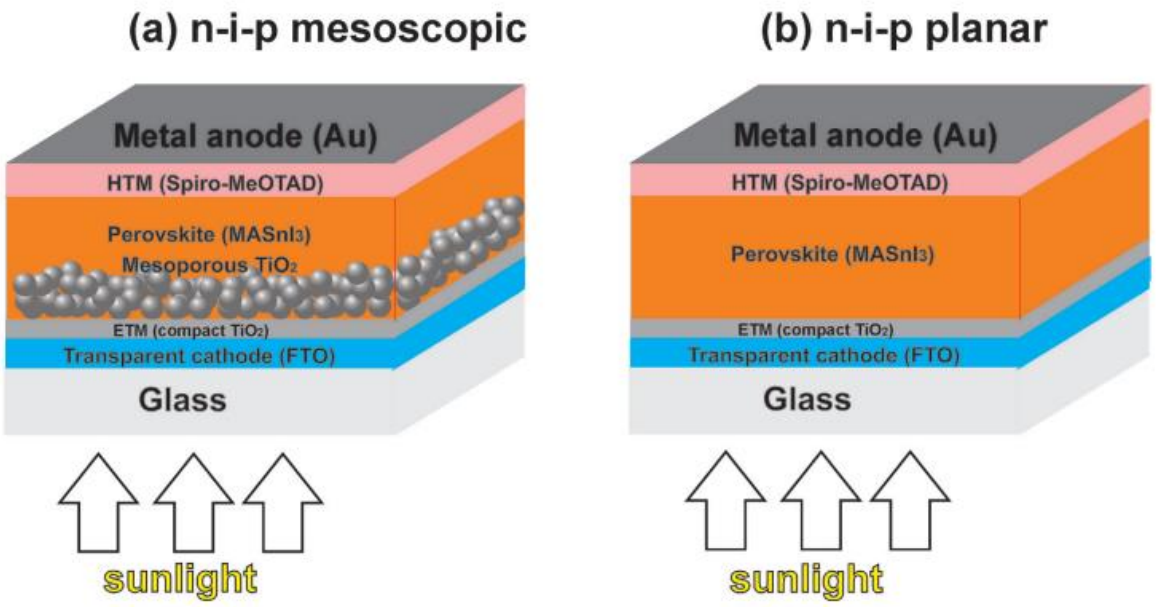

Figure II.7 : Design of perovskite solar cell A) n-i-p mesoscopic and B) n-i-p planar.

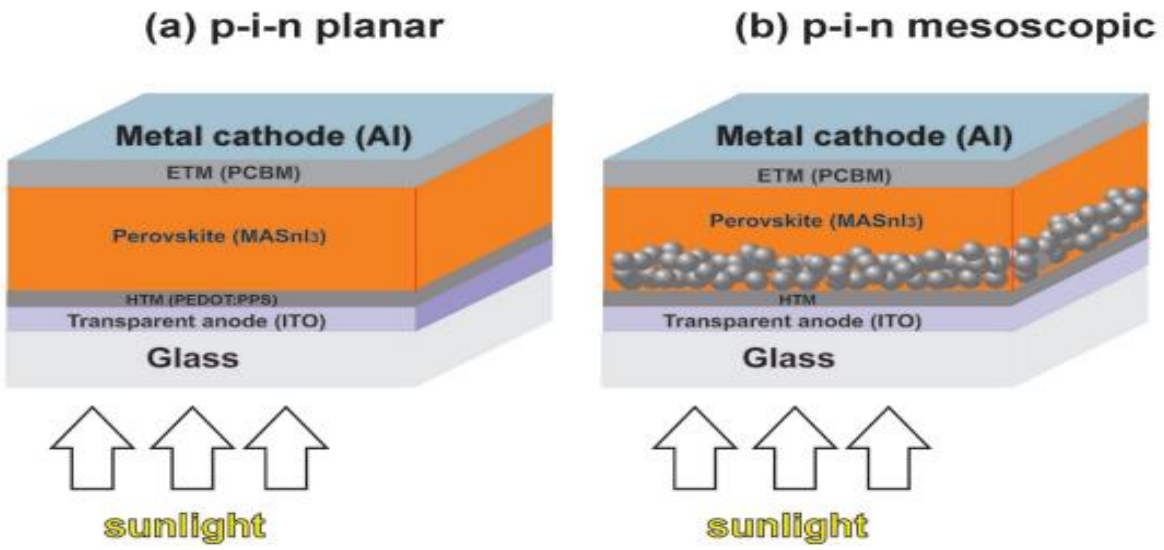

Figure II.8: Design of perovskite solar cell A) p-i-n mesoscopic and B) p-i-n planar.

2.8. Defects in the perovskite structure

Defects in perovskite materials can result from cation insufficiency in A or B sites as well as from oxygen insufficiency and/or excess. A general overview of point defects in crystals is described in the following paragraph [35].

2.8.1. Description of defects in crystals

In crystallography, point defects are defects in the organization of crystals that concern only isolated nodes [36].

2.8.2. Point defect

In the simple case of an ordered crystal AB, several types of defects can be described which are shown in Figure II.5.

- **Gap:** a gap (vacancy); it is the absence of an atom. For example, a cationic gap has a negative charge in the crystal.
- **Interstitial:** The presence of an atom in the lattice between atoms. The presence of a foreign atom between the atoms of the network is called interstitial solid solution.
- **Substitution:** The presence of a foreign atom in place of an atom in the lattice is called a solid solution of substitution.
- **Electrical charge failure:** A site of the crystal has a negative (free electron) or more positive (electron hole) charge than other sites of the same type.
- **Anti-site defects:** If the crystal is an ordes crystal, that is to say formed of several types of atoms with strict chemical alternation; then there may be anti-site defects, that is to say atoms which are well at a node of the network but which break the chemical regularity.

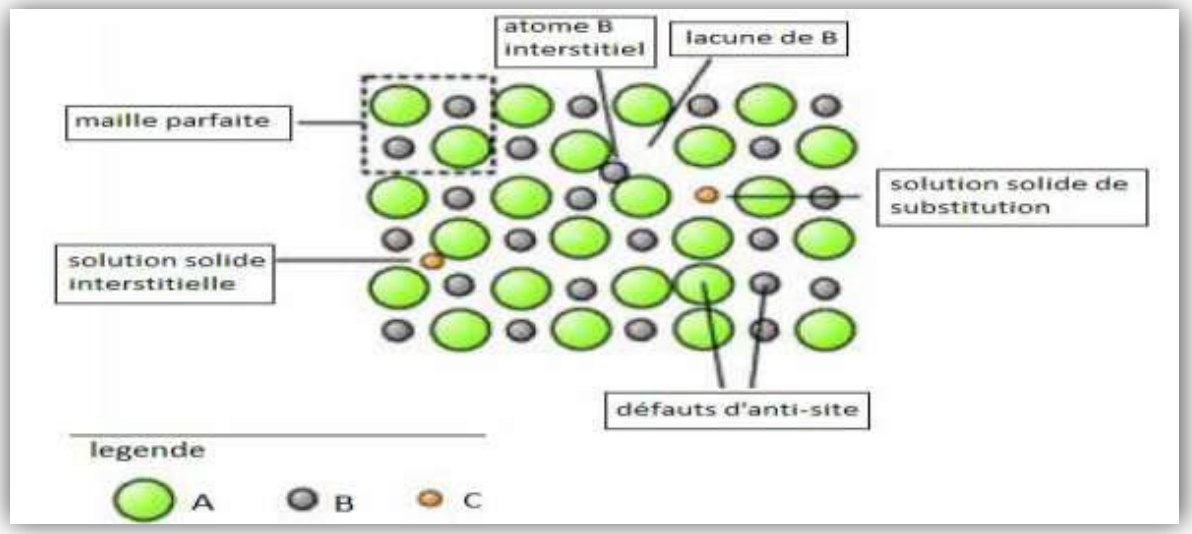

Figure II.9: Example of point defects in an ordered crystal AB.

2.9. Operating principle of Solar cells

Their operating principles have not been explained satisfactorily because of the different layers of materials involved in their manufacture, and may be different depending on their exact structure. It is assumed that the perovskite layer is excited during illumination, producing an electron-hole pair. The charge carriers can then diffuse to an interface where the electrons are injected into the conduction band (CB) of the ETL while the holes are transported to the valence band (VB) of the HTL. Finally, the electrons and holes are collected by the conductive electrodes (figure II.10). The process is thermodynamically favourable when the energy levels of the VB and CB layers align so that electron transport moves to a lower energy level while hole transport moves to higher energy levels [36].

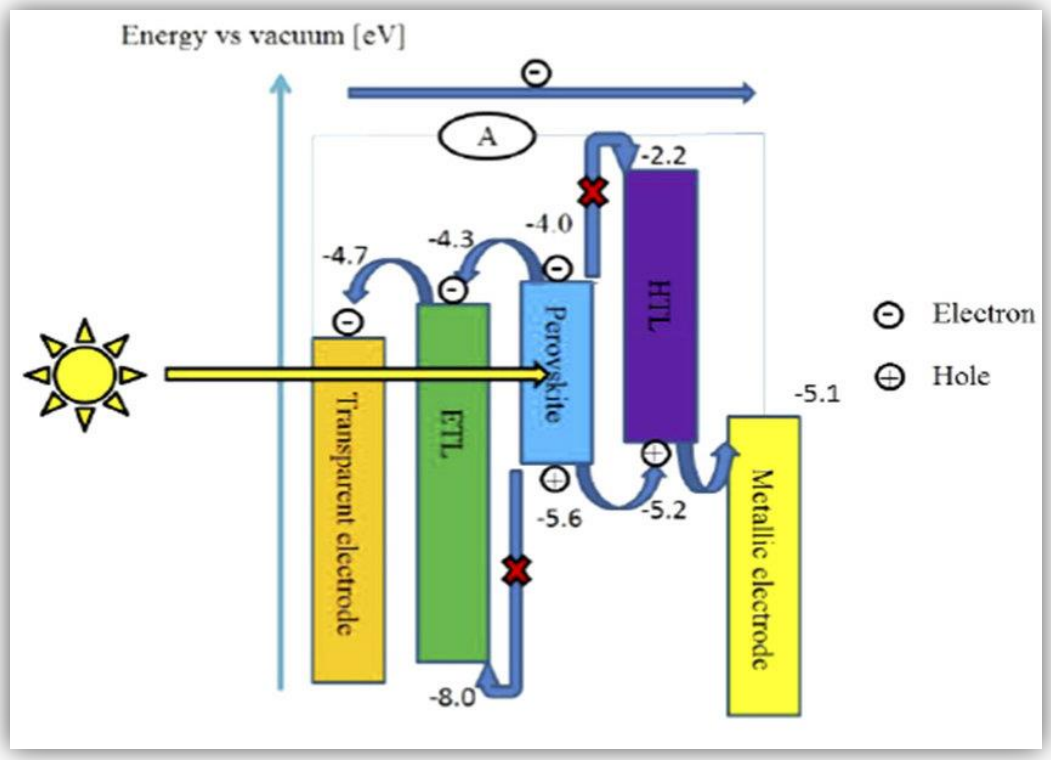

Figure II.10: Schematic of the operational principle of perovskite solar cell

The success of the perovskite layer as a solar absorber largely depends on the long length of the charge diffusion, the high mobility of the carriers in the perovskite layer and its thickness. The scattering length of electrons and holes can reach 1 μm, which is more than sufficient for photo-generated charges to reach the interfacial layers and electrodes without recombination, depending on the morphology of the perovskite layer. On the other hand, there are several recombination processes that limit the performance of the perovskite cell such as: Electrons injected into the CB of the ETL can be captured by the VB of the perovskite layer or the HTL. All charge transfer/recombination processes have been shown in Figure II.11 [37].

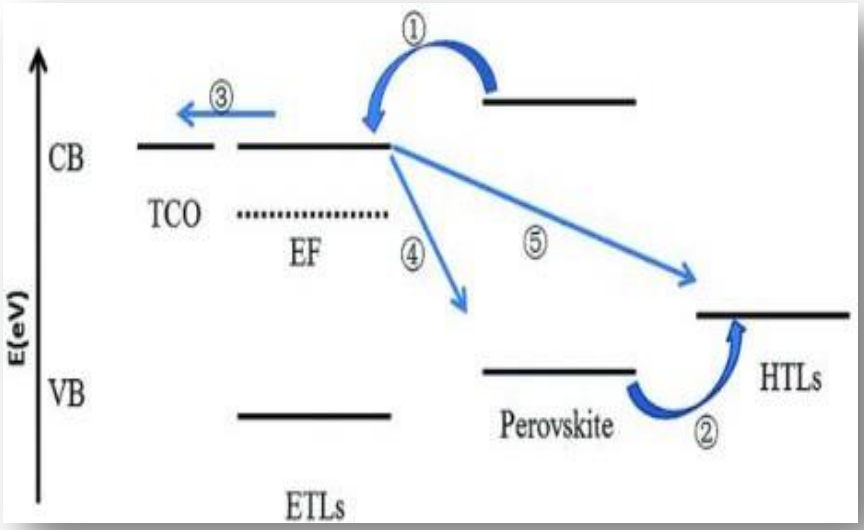

Route 1: electron injection

Route 2: hole injection

Route 3: electron transport and collection

Route 4: charge recombination at the interface between ETLs and Perovskite

Route 5: charge recombination between electrons in ETLs and the hole in HTLs

Figure II.11 : Process of charge transfer/recombination in perovskite cells

The charge transport channels in the solar cell are often discussed depending on the device structure. In the mesoporous structure, the perovskite layer is formed on a porous metal oxide (TiO2) semiconductor that creates an interpenetration network between the two phases, and therefore, the generated photo electrons can be transported along the titanium oxide domain to the FTO while the holes are transported along the perovskite

layer domain to the HTM (Figure II.12(a)). So, in the case of a planar structure, devices are made using buffer layers of ETL and HTM through which photo-generated charges created in the perovskite layer, may be directed to the electrodes when the carrier charge scattering length is greater than the thickness of the perovskite layer (Fig. II.12(b)).

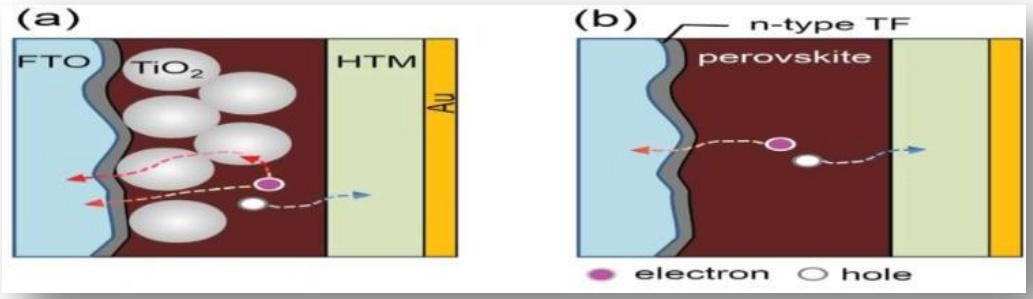

Figure II.12 : Process of charge transport in cells with perovskite (a) mesoporous structure, (b) planar structure.

In both cases, the solar energy conversion efficiency of the devices is strongly dependent on the quality of the morphology of the perovskite film. In addition, the formation of an ohmic contact between the perovskite layer and ETL/HTL is a critical factor for successful charge collection.

2.10. Comparison of the performance of some perovskite cells

The performance of solar cells based on perovskite materials depends on several parameters, such as the cell architecture, the materials used for the active layer, the layers for the transport of ETM electrons and for the transport of HTM holes and the type of electrodes as well as manufacturing techniques and conditions.

The following table gives the performance of some new generation cells based on perovskite materials.

Structure de la cellule	J_{CC}	V_{CO}	FF	η
FTO/TiO_2/$CH_3NH_3PbI_{3-x}Cl_x$/spiro-OMeTAD/Au	15.3	0.8	55	6.7
FTO/SnO_2/TIO_2/$MAPbI_{3-x}(Ac)_x$/Au	23.68	1.06	68	17.07
FTO/TiO_2/$CH_3NH_3PbI_3$: ITIC/Po-Spiro-OmeTAD/Au	23.74	1	72.8	17.59
FTO/TBD-TiO_2/$MAPbI_3$/Spiro-OMeTAD/Au	20.5	1.05	63.1	13.9
FTO/TT-TiO_2/$MAPbI_3$/Spiro-OMeTAD/Au	23.2	1.1	68	17.4
ITO/SnO_2/$MAPbI_3$/spiro-OMeTAD/Au	22.01	1.05	69	15.98
ITO/SnO_2/$MAPbI_3$-$(Gua_{1-x}MA_x)PbI_3$/spiro-OMeTAD	22.46	1.1	75	18.54
FTO/TiO_2/$CH_3NH_3PbI_3$/rGO/FTO (rGO pur)	15.86	0.71	45	5.10
FTO/TiO_2/$CH_3NH_3PbI_3$/B-rGO/FTO (10% de bore	15.91	0.71	56	7.09
FTO/TiO_2/$CH_3NH_3PbI_3$/B-rGO/FTO (20% de Bore)	16.74	0.88	60	8.96
ITO/PEDOT:PSS/ $CH_3NH_3PbI_3$ ($MAPbI_3$)/ PCBM/BCP/Al.	18.94	1.01	74.01	14.6
ITO/$AuCl_{3-GR}$/PEDOT:PSS/ $CH_3NH_3PbI_3$ ($MAPbI_3$)/ PCBM/BCP/Al.	20.13	1.01	77.53	15.77

2.11. Advantages of hybrid perovskites

Hybrid perovskites and their derivatives give better optical and structural properties. The advantages of these hybrid materials are enormous. They are easy to develop through simple and inexpensive techniques. In addition, it is possible to combine the properties of different organic and inorganic constituents, the flexibility of the organic part, the thermal stability and rigidity of the inorganic part, in a single material or even through cooperative effects, to obtain properties that are more than the simple sum of initial properties: this is organic/inorganic synergy.

Therefore, one of the main structural characteristics of these hybrids is that they can be split into thin layers through simple and inexpensive deposition techniques.

While in these hybrids the organic part may have non-linear optical properties, most of the physical properties come from the inorganic part, such as the semiconduction of iodostannate sheets, the electron transport properties, optical properties (photoluminescence, photochromism,...), or also magnetic and electrical [37].

2.12. Conclusion

In this chapter we have conducted a thorough research on perovskite-based solar cells, which possess remarkable optical and electronic properties. These different properties make hybrid perovskite a remarkable material for photovoltaic applications.

CHAPTER III:

PRESENTATION OF THE SCAPS-1D SOFTWARE

Chapter III

Presentation of the SCAPS-1D Software

3.1. Introduction

With the advancement of numerical models, numerical simulation has become a reliable and effective tool over the years for studying and understanding the behavior and characteristics of solar cell devices. These models have significantly contributed to a better understanding of the internal mechanisms of solar cells, which in turn has helped improve their efficiency and overall porfrmance.

In this chapter, we will first present the mathematical equations used to describe the operation of solar cells . Then, we will introduce the solar cell simulation software (SCAPS) that was used in our work

3.2. Fundamental equations

To accurately model the electrical properties of solar cells, SCAPS software numerically solves the basic semiconductor equations using the drift-diffusion approximation..[38]

3.2.1. Poisson equation

Poisson's equation is used to describe the relationship between potential and spatial charge

$$\frac{\partial \emptyset}{\partial x} = q\varepsilon[n(x) - p(x) - N_D^+ + N_A^- - p_t(x) + n_t(x)]$$

φ :is the potential

q: is the elementary charge

ε :is the permittivity

n: is the density of free electrons

p: is the density of free holes

N_D: is the donor doping density

N_A: is the acceptor doping density

p_t: is the density of hole traps

n_t: is the density of electron traps

3.2.2. Continuity equations

These express the conservation of carriers in a semiconductor. There are two:

One for electrons (a minority in a P basis)

One for holes (a minority in an N basis)

for the electrons:

$$\frac{\partial n}{\partial t} = \frac{1}{q}\nabla.J_n + G - R_n$$

for the holes :

$$\frac{\partial p}{\partial t} = \frac{1}{q}\nabla.J_p + G - R_p$$

n, p : concentrations of electrons and holes.

J_n, J_p : electron and hole current densities.

G: carrier generation rate by light (photons).

R : recombination rate (Shockley-Read-Hall, Auger, etc.).

q: elementary charge.

In steady state (no time dependence):

$$\nabla.J_n = q(G - R)$$

$$\nabla.J_p = -q(G - R)$$

Current shapes (drift-diffusion model):

$$J_n = -qn\mu_n\nabla\Psi + qD_n\nabla n$$

$$J_p = -qp\mu_p\nabla\Psi + qD_p\nabla p$$

3.3. Diffusion length

is the average distance a minority carrier (electron or hole) can travel before recombining.

General formula:

$$L = \sqrt{D.\tau}$$

D: Diffusion coefficient (in cm²/s

τ: Minority carrier lifetime (in seconds)

L: Diffusion length (in cm)

In the P zone, the electrons are in the minority → their diffusion length is

$$L_{n=}\sqrt{D_n.\tau_n}$$

In zone N, holes are in the minority → their diffusion length is

$$L_{p=}\sqrt{D_p.\tau_p}$$

3.4. Logical SCAPS

The simulation of thin-film solar cells has become increasingly popular in recent years, and several computational and simulation software programs have been developed by the research community in this field. These include AMPS-1D, PC-1D, ASA, SCAPS-1D, and SILVACO.

SCAPS-1D, an acronym for "Solar Cell Capacitance Simulator One Dimension," is a program developed at the University of Ghent in Belgium using Windows/CVI National Instruments by Marc Burgelman et al. This program is specifically designed for the simulation of photonic devices such as CdTe and CIGS cells [39].

SCAPS-1D's main advantages include:

- Input files are accessible to the user in text format, including spectral data and device parameters.
- The ability to introduce interfaces and take into account the recombination phenomenon. *Introduction of series resistors and obtaining capacitance-voltage and capacitance-frequency characteristics.
- This software offers high execution speed.

3.5. SCAPS 1D Software Interface

is the graphical environment that allows the user to set simulation parameters, define the solar cell structure, run calculations, and analyze results through various functional windows and panels (figure1).

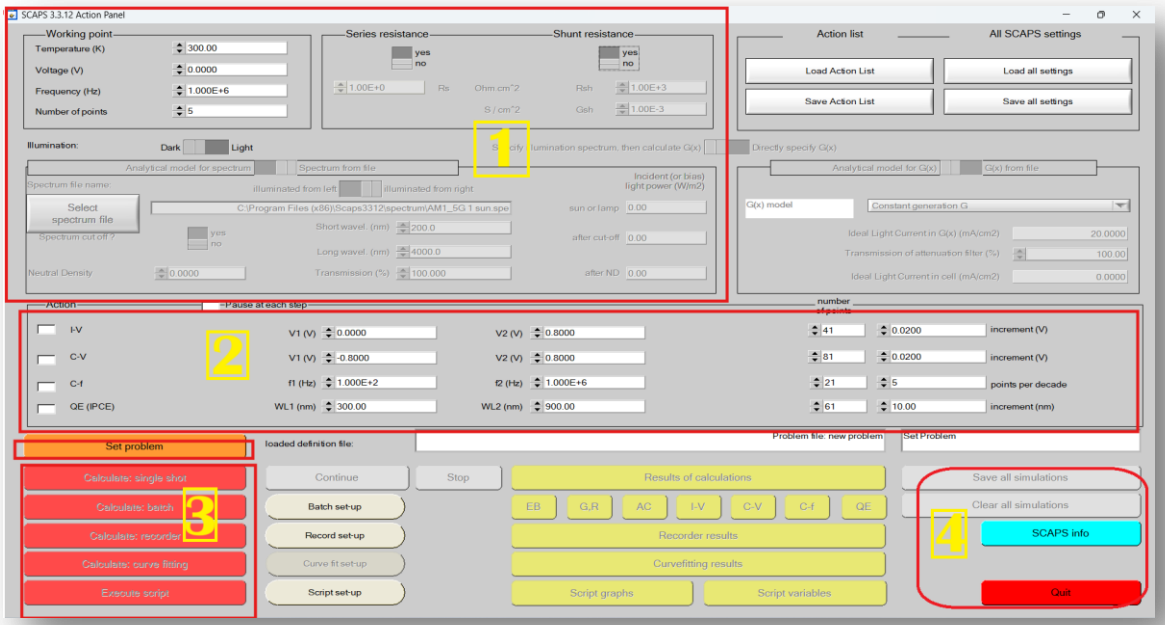

Figure III.1 : Execution Window <Action Panel> of the SCAPS

(1). Working Point and Illumination Settings:
This section defines the experimental conditions, such as temperature, voltage, frequency, and number of data points. It also allows the selection of the illumination spectrum used for the simulation, whether artificial or solar.

(2). Action and Range Settings:
This part is used to select the type of simulation (I-V, C-V, C-f, or QE) and to specify the start and end values of voltage, frequency, or wavelength, along with their increments, depending on the chosen simulation.

(3). Calculation Execution Options:
This section contains buttons to execute different types of simulations: single calculation, batch mode, scan mode, curve fitting, or script execution. It allows launching simulations after defining the problem.

(4). Results and SCAPS Info Section:
This area provides options to save or clear simulation results. It also includes access to SCAPS info and allows exiting the software or continuing to other configurations.

3.5.1 Defining the Operating Point:

The operating point specifies the parameters that are not variable in the simulation measurements and that are relative to the measurement operation. This includes:

- Temperature T: Important for all measurements. Note: In SCAPS: Nc(T), Nv(T), thermal velocities, thermal voltage kT, and all their derivatives are the only variables that have an explicit thermal dependence; the corresponding material parameters must be manually entered for each T value.
- Voltage V: This does not apply to I-V and C-V simulations. It is the DC bias voltage in a C-f and QE(λ) simulation. SCAPS always starts at 0 V and runs at the operating point voltage through a number of steps that must also be specified.
- Frequency f: This does not apply to I-V, QE(λ), and C-f simulations. This is the frequency at which the C-V characteristic is simulated.
- Number of points: The number of points used to plot the curves.

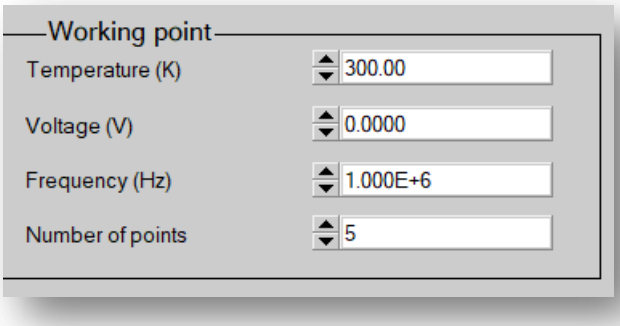

Figure III.2 : the Operating Point

❖ **L'illumination**

It is used in all measurements. For QE(λ), it determines the polarization conditions of the light. The basic parameters are: darkness or light, choice of illuminated side, and choice of spectrum. The illumination spectrum on Sun (= 1000 W/m2) with a global air mass of 1.5 is the default spectrum, but a wide range of monochromatic lights and spectra are also available for more custom simulations. If an optical simulator is available, a generation profile can be immediately loaded instead of using a spectrum.

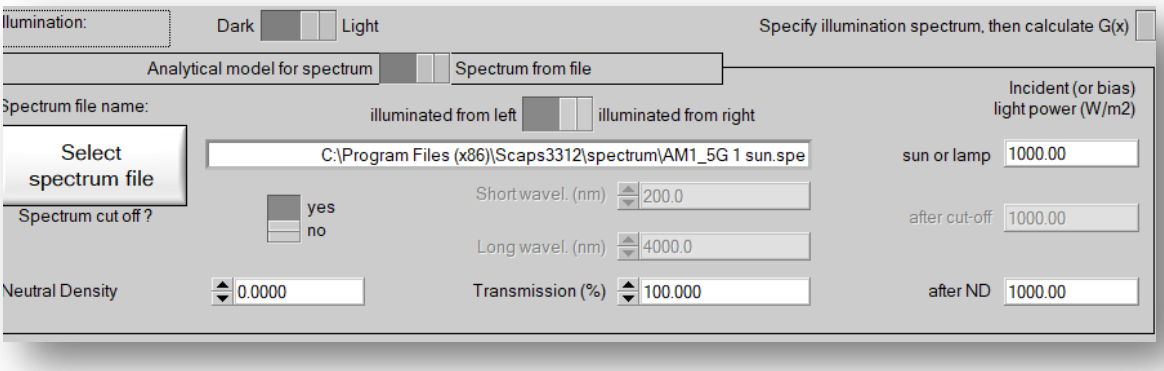

Figure III.3 : L'illumination.

3.5.2. Selecting the characteristics to simulate:

In the Action section of the action panel, you can select one or more measures to simulate: IV,

C-V, C-f, and QE(λ). You can also adjust the initial and final values of the argument, as well as the number of steps.

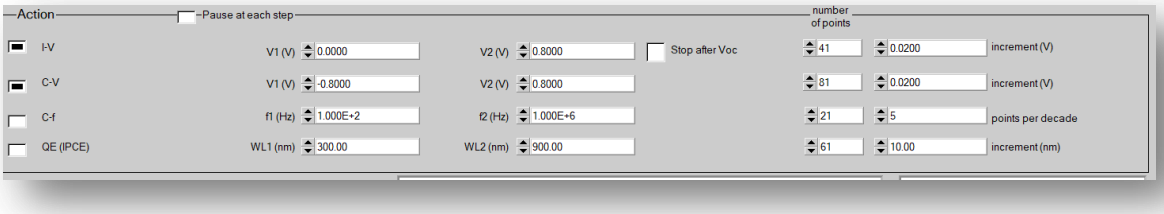

Figure III.4 : Configuration of the parameters to be simulated.

3.5.3. Device Design Window (Set Problem):

When we enter the "Problem Setting" area, the following window appears, where there are a set of sections that we will discuss to explain each section:

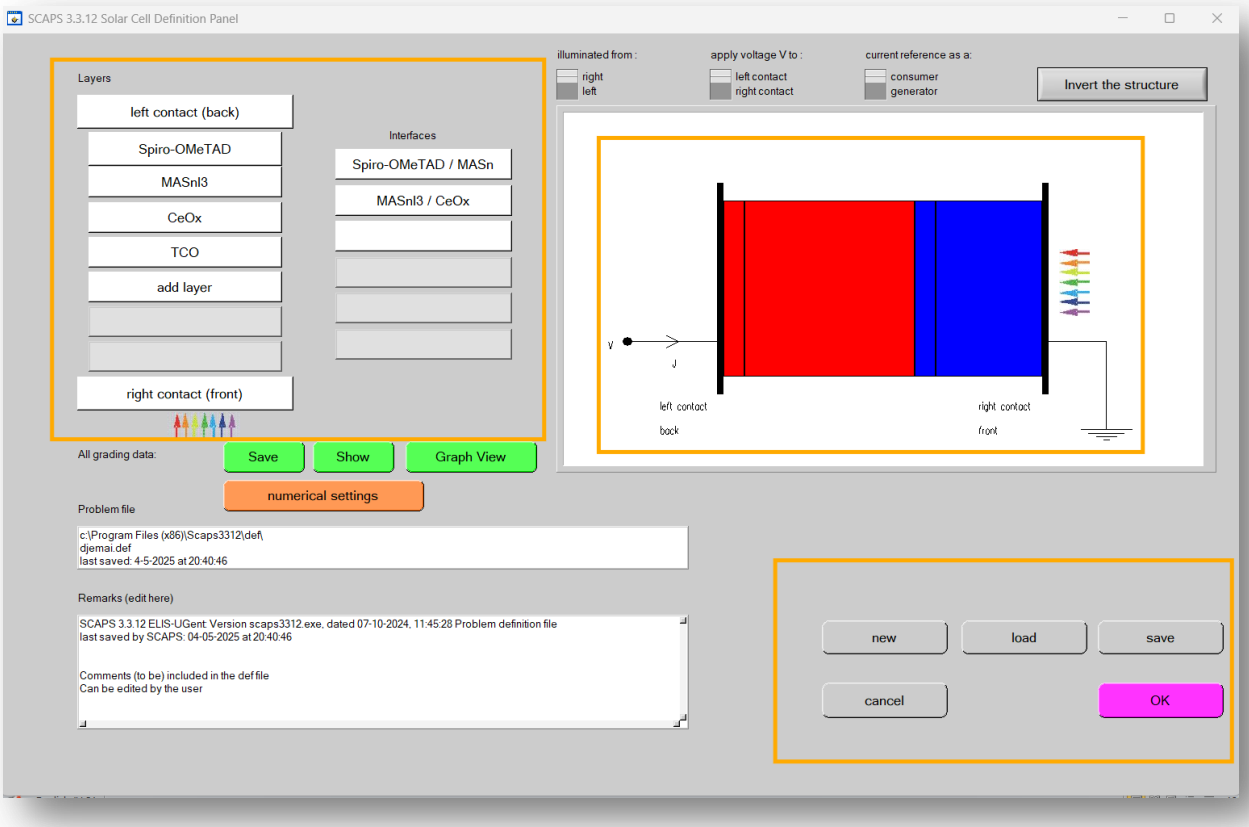

Figure III.5 : Solar cell layer definition interface.

3.5.3.1. Solar Cell Structure Editing:

When the "SET PROBLEM" button is clicked within the action panel, the "SOLAR CELL DEFINITION" panel will be displayed. This panel allows users to create or modify solar cell structures, as well as to save new structures or load existing ones from definition files.

These definition files are stored in ASCII (American Standard Code for Information Interchange) format and carry the .def extension. They can be opened using simple text editors such as Notepad.exe or Wordpad.exe. However, it is strongly recommended not to manually edit these files, as improper modifications may render them unusable by the program.

The properties of the layers, contacts, and interfaces can be modified by clicking the corresponding buttons, as illustrated in Figure II.6. Similarly, additional layers can be added to the solar cell structure by clicking the "ADD LAYER" button.

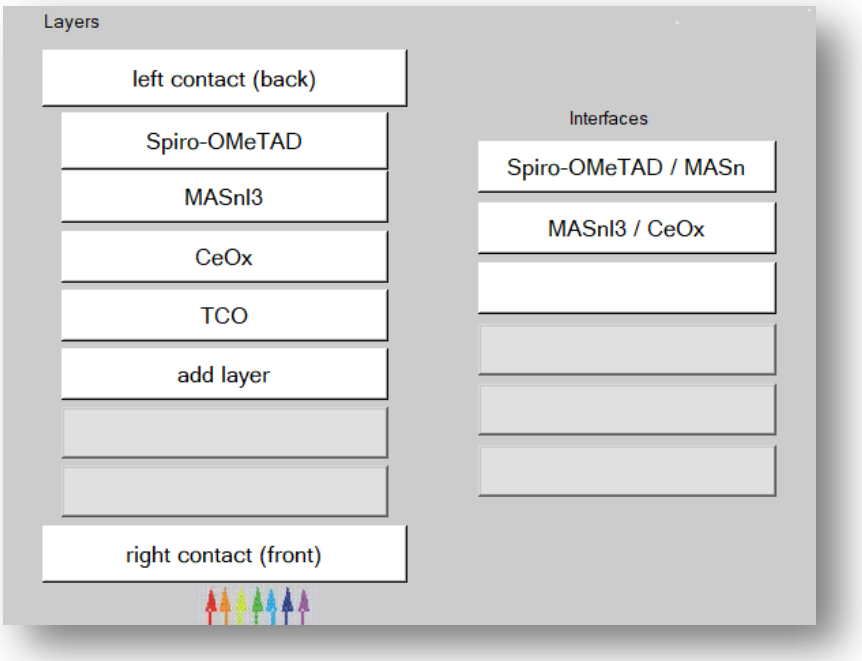

Figure III.6 : Definition of the structure of a solar cell

A. Defects

Defects can be defined using the "add defect" button located in the layer properties definition panel. This panel also allows the specification of recombination models associated with the defects.

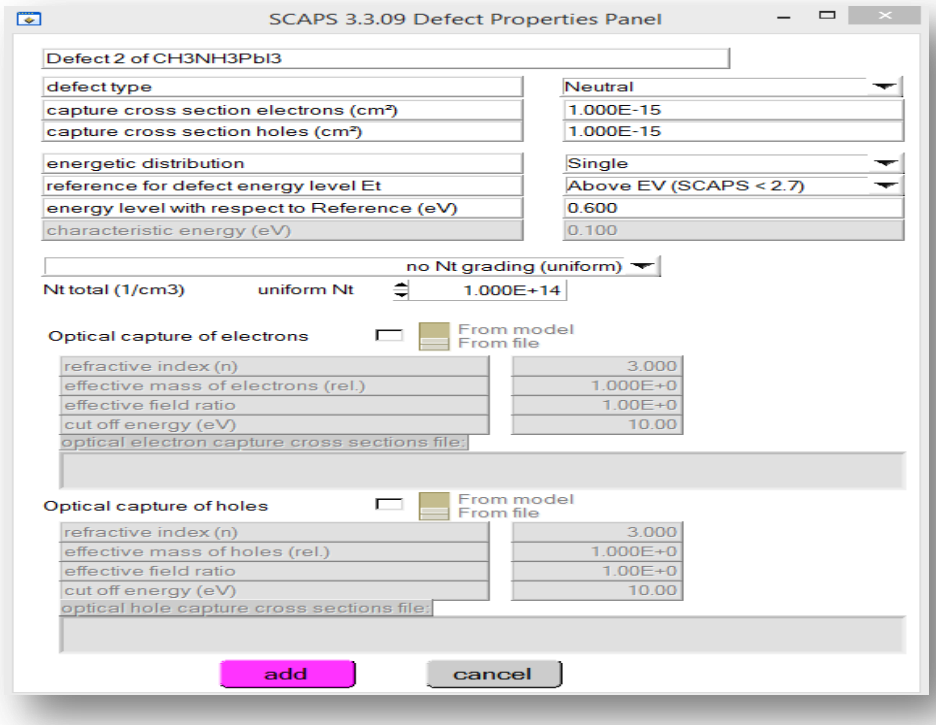

Figure III.7 : Default property definition panels.

B. Contacts

Contact properties can be entered by clicking either the front contact button or the back contact button on the cell definition panel.

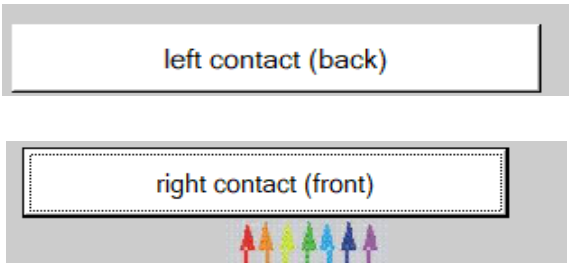

A 'CONTACT PROPERTIES PANEL' opens, as shown in **Figure8** .

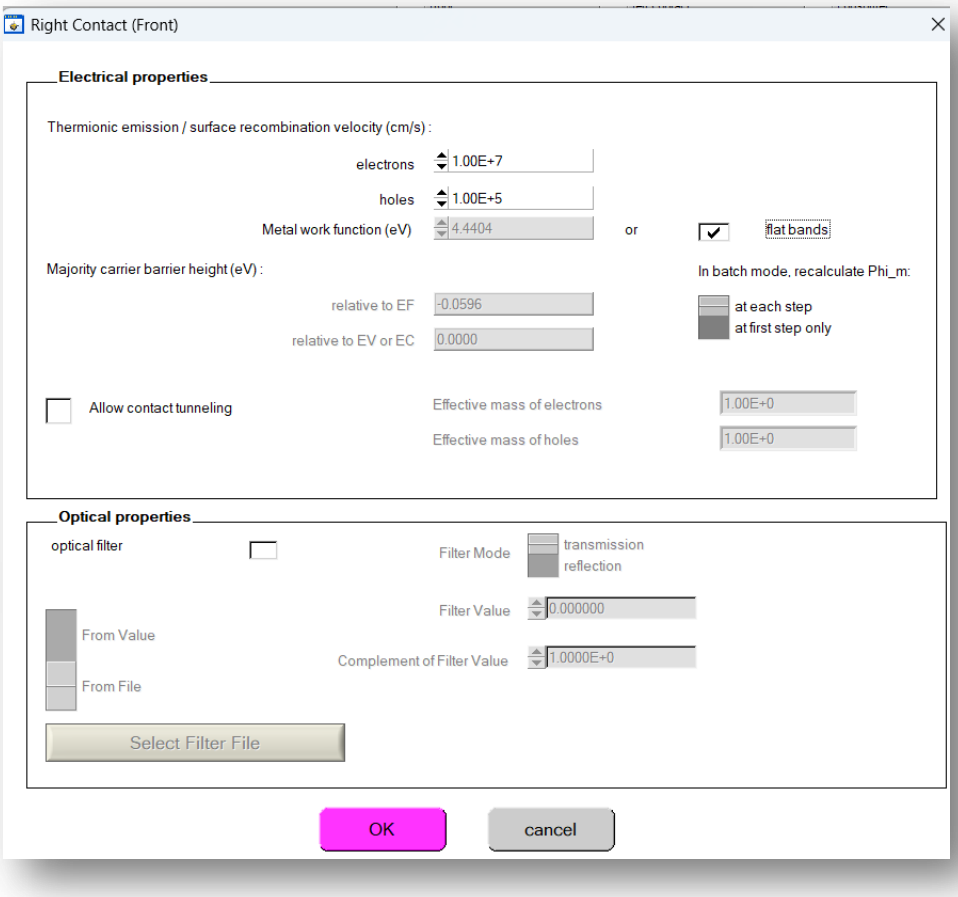

Figure III.8 : Contact Properties Panel.

❖ Electrical Properties

Surface Recombination Velocity of Electrons and Holes: Describes how quickly free electrons and holes recombine at the contact surface, leading to a loss of charge carriers. Work Function or Flatband Condition: Determines whether the contact generates an energy barrier (work function) or if it is ideal with no barrier (flatbands).

Majority Carrier Barrier: The amount of energy that majority carriers (electrons or holes) need to overcome to cross the contact.

Tunneling: A quantum phenomenon where carriers can pass through an energy barrier without needing enough energy to surmount it; can be considered or ignored depending on the model.

Optical Properties: Light transmission or reflection at the contact can be defined either by a constant value or through a detailed data file

C. Layer Definition

By clicking the "add layer" button, opens containing the various material parameters to be entered. These parameters can have uniform or non-uniform distributions, depending on the material's physics.

In the first box, the layer name is entered (which corresponds to the doping type).

In the second box, the layer thickness is entered.

The third block concerns the material's purity and profile.

In the fourth block, the following are entered: the energy gap, electron affinity, dielectric permittivity, effective densities of the conduction and valence bands, thermal velocities of free electrons and holes, and electron and hole mobilities. Finally, a box allows the addition of the effective masses of electrons and holes if carrier transport by tunneling is taken into account. If the material is a compound of elements with non-uniform concentrations, gradual variations of the previous parameters can be introduced.

In the fifth block, we introduce the doping, type, and density. Doping can also be introduced as uniform, as it can have gradual variations (linear, parabolic, etc.).

In the sixth block, the absorption of the layer is defined, Absorption can be defined by the analytical model provided by SCAPS, or it can be entered as data. SCAPS provides a number of absorption data for several types of semiconductors. Other absorption data for semiconductors not available in SCAPS can also be used, provided the file has the same extension as the absorption files provided by SCAPS.

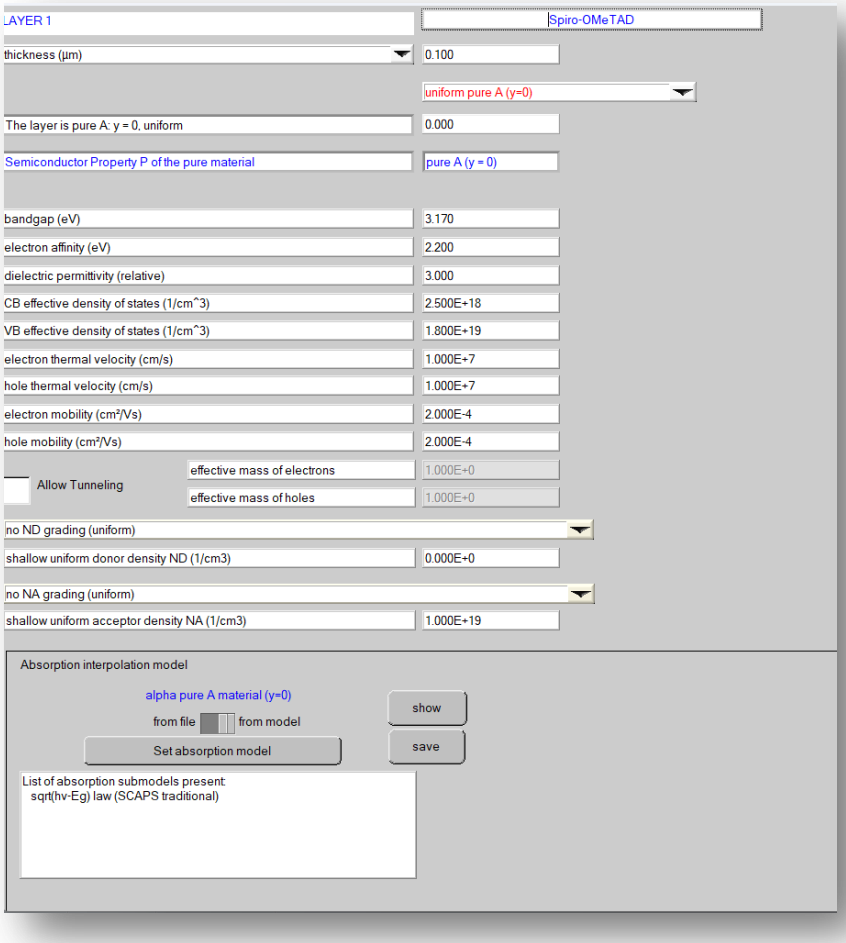

Figure III.9 : Properties of the added layer.

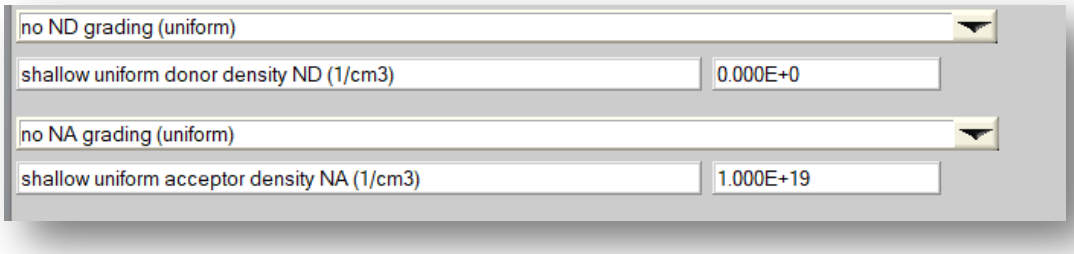

Figure III.10 : Properties of the defined dopings.

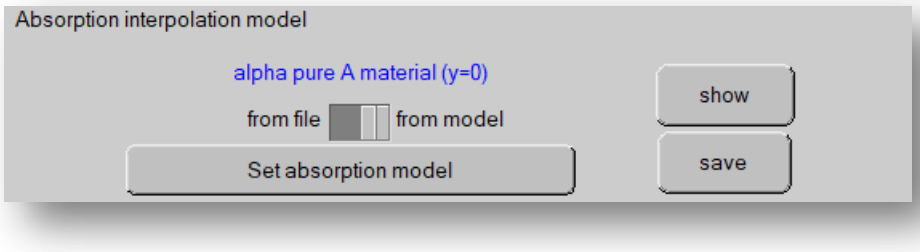

Figure III.11 : Absorption mode

3.5.3.2. Define the problem

1. Save : to save the cell to be studied.
2. Load : to select a previously saved cell.
3. OK : to approve the constructed cell and return to the action panel to finish the work.
4. Cancel : to decline the definition panel and return to the action panel.

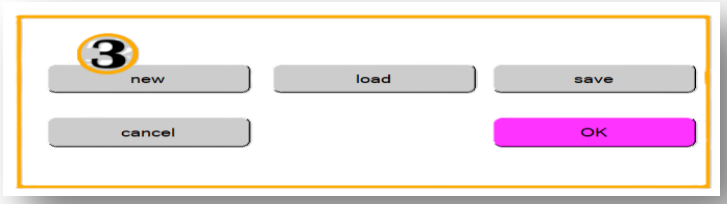

Figure III.12 : Define the problem.

3.5.3.3. display of the PV

is a display of the defined structure of the device photovoltaic with front and back contacts. There are also additional buttons for selecting device illumination from either the back or front contact side, the direction of voltage applied to a device, and finally a button dedicated to reversing the order of the structure layers.

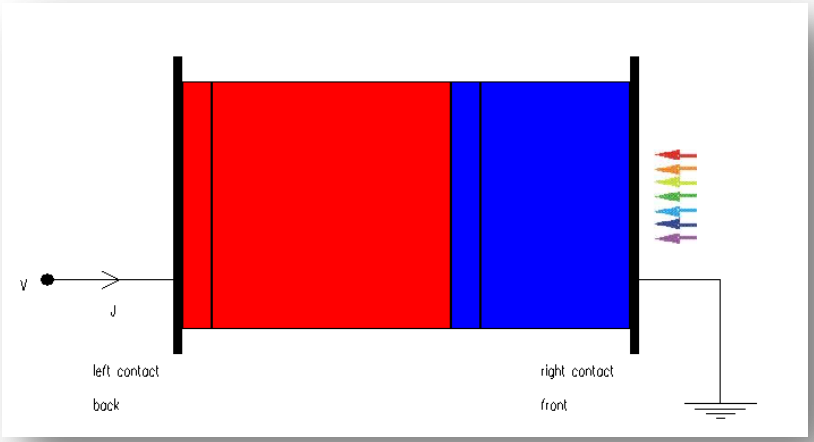

Figure III.13 : display of the PV device to be simulated

❖ **Start The Calculation**

Click on <<calculate: single shot>> to start the simulation.Start the calculation.

3.5.4. Displaying Simulated Curves

After the calculations are completed, SCAPS automatically moves to the energy band diagram panel, as shown in Figure III.2. In this panel, you can view the band diagrams, the densities of free carriers, and the current density at the last calculated bias point.If you wish to display results at intermediate voltage points, you can use the "pause" button in the action panel. Results can also be displayed using the "PRINT," "SAVE GRAPHS," and "SHOW" commands, with the corresponding values appearing on the screen.It is possible to copy and paste thers into paste the results into other applications, such as Excel, or to save them into a data file[39].

Additionally, you can switch to one of the customized panels, provided that at least one measurement simulation has been previously performed.

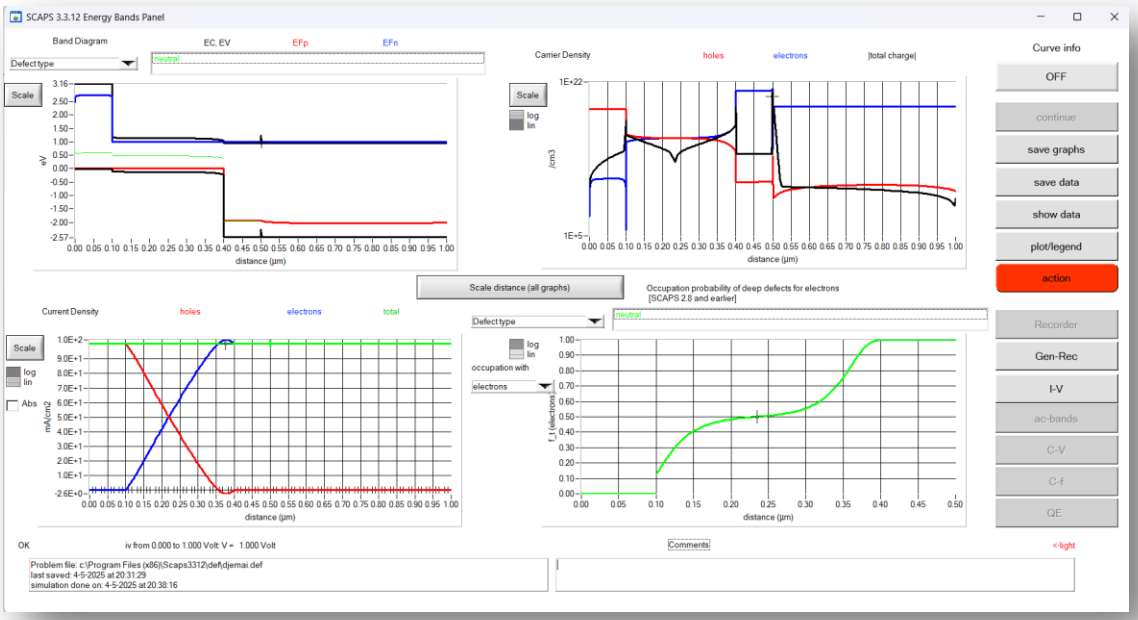

Figure II1.14 : Energy bands panel.

3.6. Curves I-V

This panel displays current-voltage (I-V) curves in two conditions: dark and light. Here are some important details to note:

Last calculated curve color: This is indicated by color in the legend, and the user can click the "Clear All Graphs" button to remove overlap in the graphs if the graph is crowded.

Recombination rate curves: These are displayed only for the last simulation, making it easier to track changes resulting from a particular simulation.

Curve Details: When the "CURVE INFO" option is enabled and a specific curve is clicked on in the chart, a pop-up panel appears containing additional information about the curve and the available points within it.

SCALE Button: Allows the user to modify the range of the axis or scale, making it easier to understand the data.

Scale Using the CTRL Key: Enlarges or reduces specific areas of the chart when selected or clicked with the mouse.

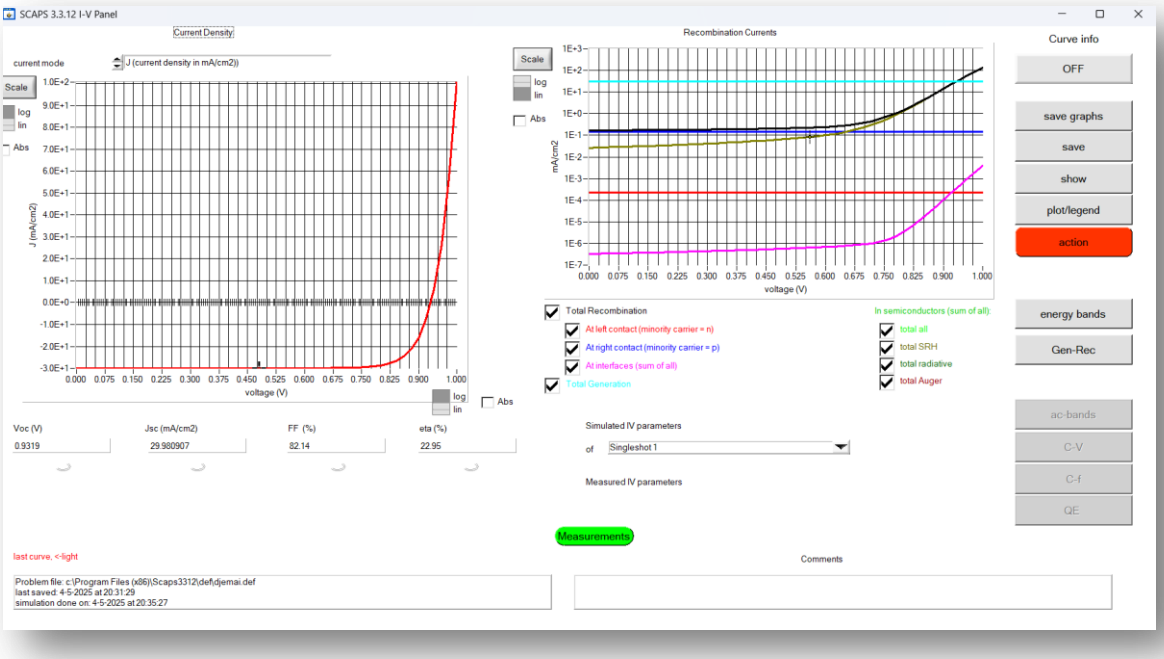

Figure III.15 : Display panel of I-V curves in illumination.

3.7. Conclusion

SCAPS-1D is a good software used for the one-dimensional numerical simulation of photovoltaic devices. This model is based on solving the electron and hole continuity equations and on the Poisson equation. It is very easy to use. In this chapter, we presented in detail the operation of this one-dimensional simulation tool, the different modules, the structure definition section, and finally the results display section. Given the advantages of this software, we chose to use SCAPS-1D to simulate a conventional structure of a CIGS-based solar cell. In the following chapter, we will present the simulation of the proposed structure, the photovoltaic performance results obtained, and the discussion.

CHAPTER IV:

SIMULATION RESULTS OF THE MASNI3 SOLAR CELL

Chapter IV

Simulation results of the MASnI3 solar cell

4.1. Introduction

In this chapter, we will study and simulate a single-layer solar cell using the SCAPS numerical simulation software. The cell is based on the hybrid perovskite material MASnI3 as the absorber layer, CeOx as the electron transport layer (ETL), and Spiro-OMeTAD as the hole transport material (HTM). Initially, we will investigate the effects of layer thicknesses on the performance of the solar cell, focusing on variations in the absorber layer thickness as well as the choice of materials for both the ETL and HTM layers. Finally, an intrinsic layer of MASnI3 was added to further enhance the performance of the perovskite solar cell.

4.2. Simulation numérique de la cellule solaire pérovskite monocouche MASnI3

Figure IV.1 shows the structure of the MASnI3-based perovskite solar cell that we will simulate. This cell consists of the layers: Spiro-OMeTAD / / MASnI3 / CeOx / TCO

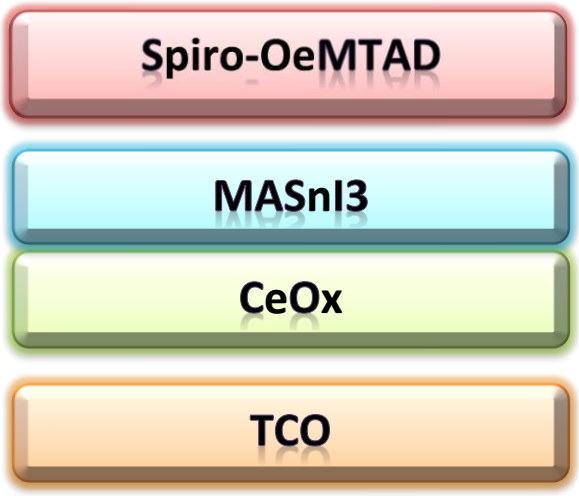

Figure IV.1 : Structure of the MASnI3-based perovskite solar cell

The cell consists of an active absorber layer made of MASnI3, an electron transport layer (ETL) composed of CeOx, and a hole transport layer (HTL) made of Spiro-OMeTAD. The cathode of the cell is formed by TCO material, while the anode is made of MoO_3. Illumination from the AM 1.5 G solar spectrum is applied to the TCO side of the solar cell.

We will begin by studying the effects of the thicknesses of the three materials—Spiro-OMeTAD, MASnI3, and CeOx—on the electrical characteristics of the cell.

Figure IV.2 shows the schematic diagram of the MASnI3-based solar cell modeled in SCAPS.

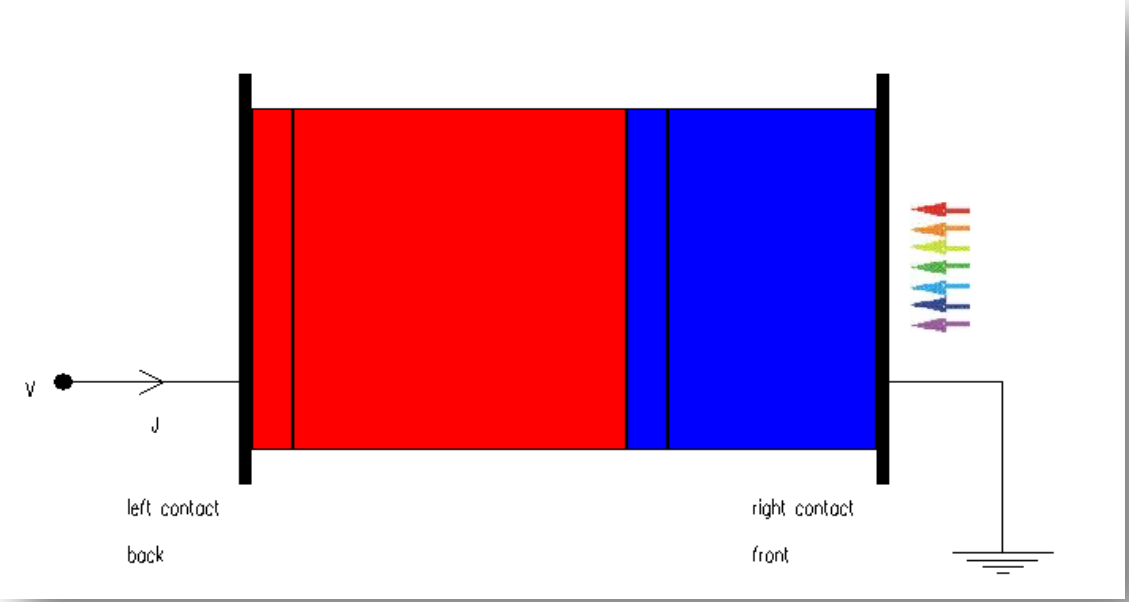

Figure IV.2 : Schematic of the perovskite solar cell simulated using SCAPS

The structural parameters as well as the physical parameters of the different layers are grouped in the following table.[40]

Table IV.1: Properties of the different layers of the solar cell (Spiro-OMeTAD,MSAnI3, CeOx, TCO).

Materials	**Spiro-OMeTAD**	**MASnI3**	**CeOx**	**TCO**
thickness (µm)	0.1	0.3	0.1	0.5
Bandgap (eV)	3.17	1.26	3.5	3.5
Electron affinity (eV)	2.2	4.2	4.3	4
Dielectric permittivity (relative)	3	8.2	9	9
CB effective density of states ($1/cm^3$)	2.5×10^{18}	1×10^{18}	1×10^{20}	2.2×10^{18}
VB effective density of states ($1/cm^3$)	1.8×10^{18}	1×10^{18}	2×10^{21}	1.8×10^{19}
Electron thermal velocity (cm/s)	1×10^{7}	1×10^{7}	1×10^{7}	1×10^{7}
hole thermal velocity (cm/s)	1×10^{7}	1×10^{7}	1×10^{7}	1×10^{7}
Electron mobility (cm^2/Vs)	2.000E-4	2	100	20
Hole mobility (cm^2/Vs)	2.000E-4	2	25	10
Donor density ND ($1/cm^3$)	0	1	1×10^{21}	2×10^{19}
Acceptor density NA ($1/cm^3$)	1×10^{19}	1×10^{10}	0	1

4.3. Electrical Characteristics of the Single-Layer Perovskite Solar Cell Made of MASnI3

4.3.1. Current-Voltage Characteristics

The electrical characteristic of the current density J(V) under illumination by the AM1.5 solar spectrum with an intensity of 100 mA/cm^2 is shown in Figure IV.3.

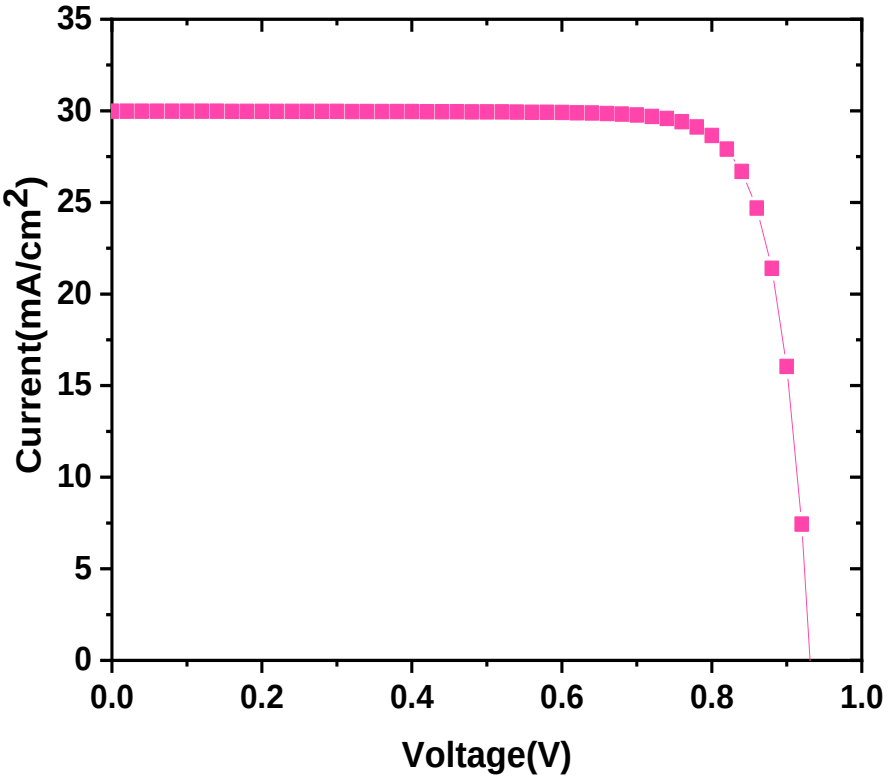

Figure IV.3 : J(V) characteristic of the perovskite solar cell.

Table IV.2 : Photovoltaic Parameters of the Monolayer Perovskite Solar Cell

Settings	**J_{sc} (mA/cm^2)**	**V_{co} (V)**	**FF (%)**	**η (%)**
Values	29.979651	0.9086	82.14	22.95

The efficiency, which is equal to 22.95%, is in good agreement with the efficiency found in the literature for a MASnI3 perovskite solar cell

4.3.2. Spectral Response

Figure IV.4 represents the quantum efficiency as a function of wavelength for the perovskite solar cell. We note that the efficiency has a maximum in a wavelength range between 360 nm and 900 nm, then it drops at low and high wavelengths. From this figure, the quantum efficiency vanishes at a wavelength of around 0.98 µm, which corresponds well to the threshold wavelength λ_{seuil} = 0.98 µm of the solar spectrum for the perovskite material MASnI3.

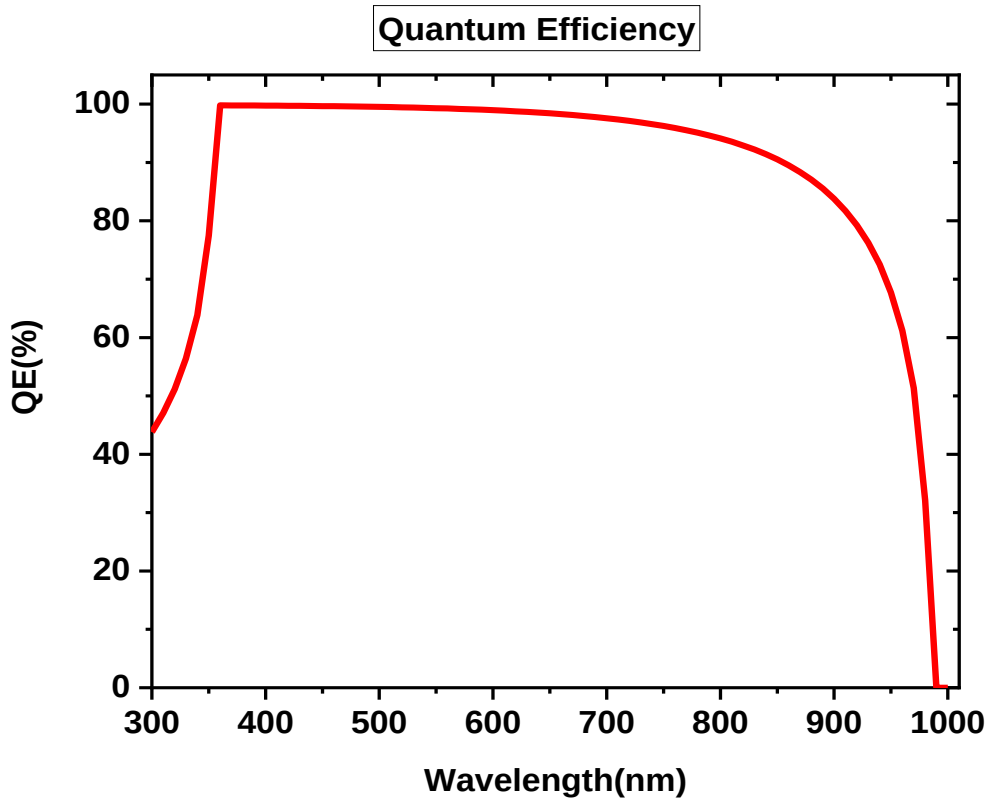

Figure IV.4 : Rendement quantique externe de la cellule solaire en pérovskite monocouche.

4.4. Effect of MASnI3 Layer Thickness on the Photovoltaic Parameters of the Solar Cell

Having an adequate perovskite layer thickness is essential to ensure maximum absorption of light passing through it, as perovskite materials possess a high absorption coefficient, making this layer the primary absorber in the solar cell structure.

In this study, we investigated the impact of varying the perovskite layer thickness on the output performance of the solar cell. The thickness was varied from 0.1 µm to 0.8 µm, while all other parameters were kept constant as shown in Table IV.1. The results obtained for(J_{sc}, V_{OC}, FF, η)are presented in the following table.

Table IV.3 : Effect of MASnI3 layer thickness on photovoltaic parameters of solar cell

thickness (µm)	$J_{sc}(\frac{mA}{cm2})$	$V_{OC}(V)$	***FF (%)***	η **(%)**
0.1	17.454538	0.9673	82.82	13.98
0.2	25.735674	0.9474	82.58	20.13
0.3	29.979651	0.9319	82.14	22.95
0.4	32.298918	0.9193	81.55	24.22
0.5	33.640871	0.9086	80.87	24.72
0.6	34.455641	0.8996	80.05	24.81
0.7	34.969823	0.8915	79.16	24.68
0.8	35.303408	0.8846	78.16	24.41

Based on the table, it can be observed that the optimal thickness for the MASnI3 layer is 0.9 µm. The short-circuit current (Jsc) increases progressively with thickness, rising from 17.45 to 35.30 mA/cm². This improvement is due to the enhanced ability of the perovskite layer to absorb longer wavelengths of light as its thickness increases. The open-circuit voltage (Voc) shows only a slight decrease with thickness, and the fill factor (FF) also drops slightly, reaching 78.16% at a thickness of 0.8 µm. Moreover, the overall power conversion efficiency improves with increasing thickness, ranging from 13.98% to 24.41%. Considering all these factors, the optimal thickness of 0.6 µm was selected, corresponding to a high efficiency of 24.81%.

Figure IV.5 illustrates the effect of the perovskite layer thickness on the performance of the MASnI3-based solar cell.

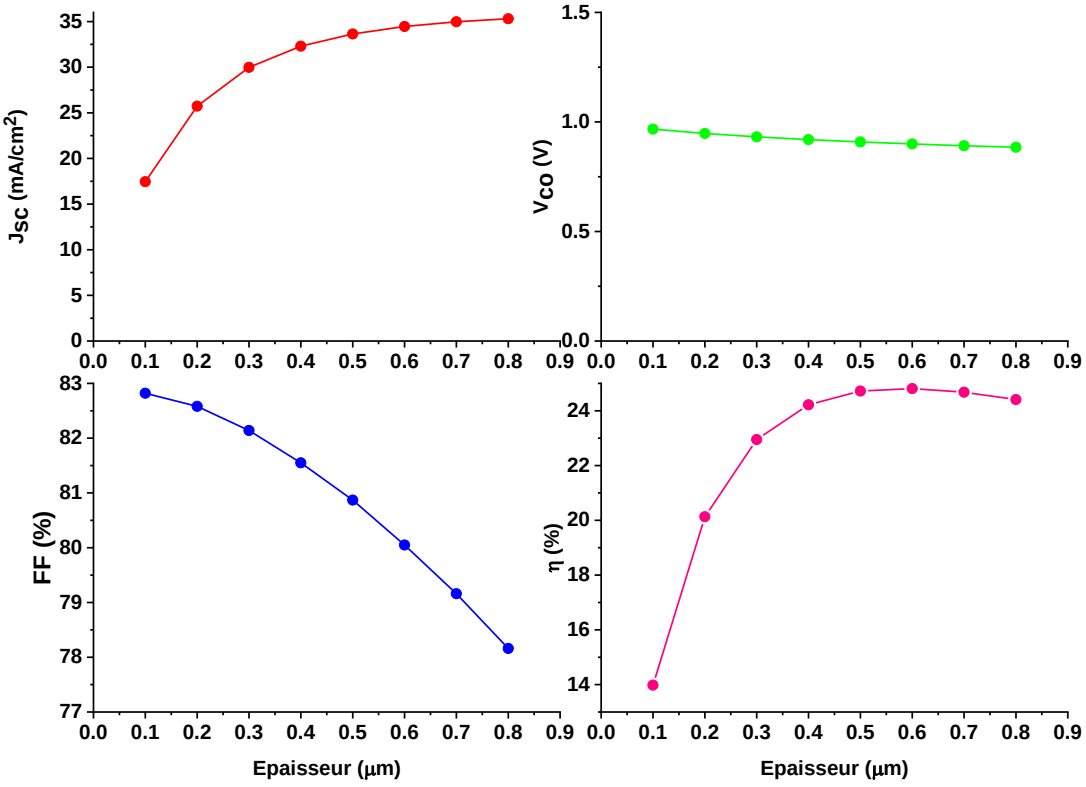

Figure IV.5 : Effect of perovskite layer thickness on solar cell performance.

The effect of perovskite layer thickness on the I-V characteristic is also illustrated and shown in Figure IV.6. We find that Jsc increases with the thickness of the perovskite layer.

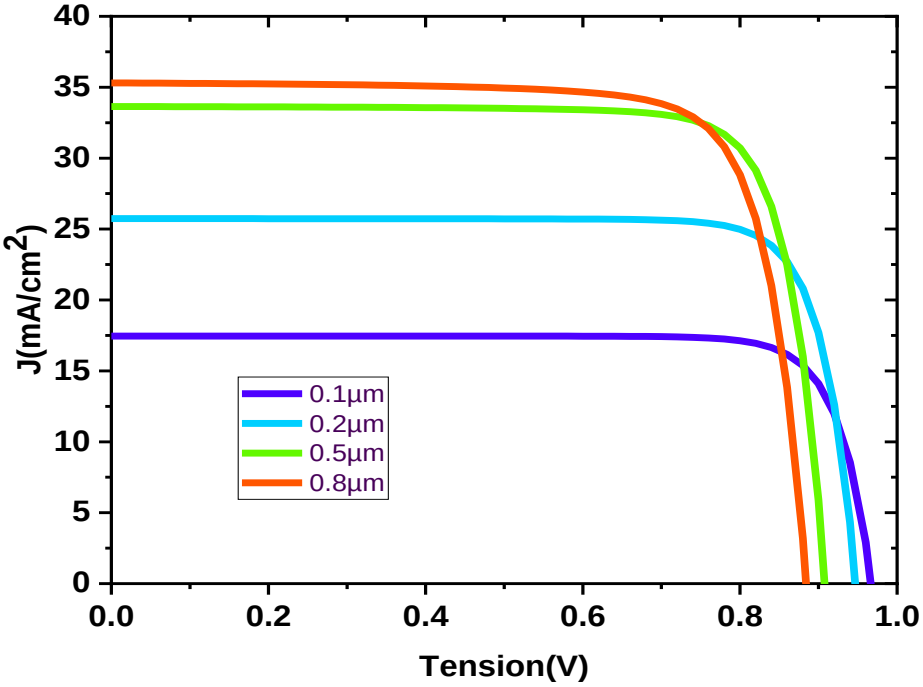

Figure IV.6 : Influence of the thickness of the MASnI3 layer on the J-V characteristics of the solar cell .

4.4.1. Effect of Spiro-MeOTAD Layer Thickness on Solar Cell Photovoltaic Parameters

In our study, we considered a perovskite layer thickness of 0.6 µm and varied the thickness of the HTL material (Spiro-OMeTAD) from 0.1 to 0.5 µm. The other parameters were set as shown in Table IV.3. The results obtained (Jsc (mA/cm^2), V_{CO} (V), FF (%) and η (%)) are shown in the following table.

Table IV.4 : Effect of Spiro-MeOTAD layer thickness on solar cell photovoltaic parameters

thickness (µm)	$J_{sc}(\frac{mA}{cm2})$	$V_{CO}(V)$	*FF (%)*	η *(%)*
0.1	34.455641	0.8996	80.05	24.81
0.2	34.455491	0.8996	79.95	24.78
0.3	34.455340	0.8996	79.84	24.75
0.4	34.455189	0.8996	79.74	24.72
0.5	34.455038	0.8996	79.63	24.68

From this table, we note that this layer has no influence on the photovoltaic parameters of the solar cell. In the following, we chose a thickness of 0.1 µm , corresponding to an efficiency of η = 24.68%.

Figure IV.7 shows the effect of Spiro-OMeTAD layer thickness on solar cell performance.

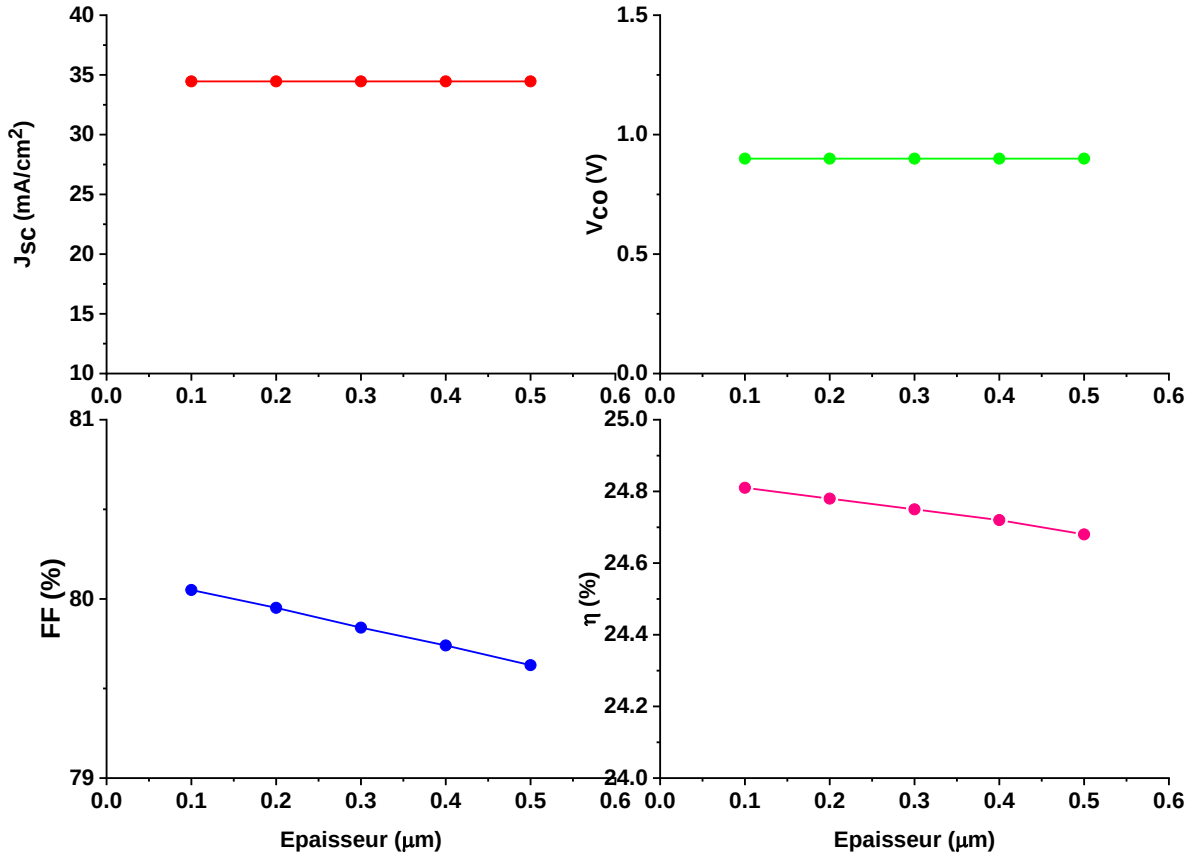

Figure IV.7 : Effect of Spiro-MeOTAD layer thickness on solar cell photovoltaic parameters.

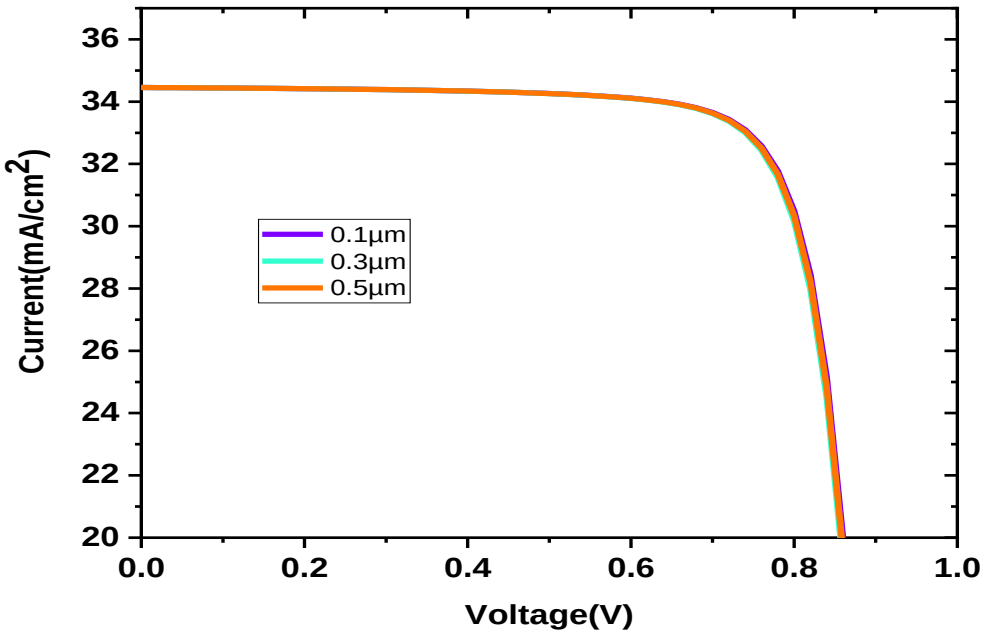

Figure IV.8 : Influence of the thickness of the Spiro-OMeTAD layer on the J-V characteristics of the solar cell

4.4.2. Effect of Spiro-MeOTAD N_A Acceptor Density on Solar Cell Photovoltaic Parameters

In our study, we considered a perovskite layer thickness of 0.6 µm and varied the NA Acceptor Density material (Spiro-OMeTAD) from 1×10^{16} to 1×10^{21}1/cm^3. The other parameters were defined as shown in Table IV.5. The results obtained (Jsc (mA/cm²), V_{OC} (V), FF (%) and η (%)) are presented in the following table.

Table IV.5 : Effect of Spiro-MeOTAD NA Acceptor Density on Solar Cell Photovoltaic Parameters

NA	$J_{sc}(\frac{mA}{cm2})$	$V_{OC}(V)$	*FF (%)*	η *(%)*
1×10^{16}	33.854568	0.8987	32.01	9.74
1×10^{17}	34.409122	0.8960	67.11	20.69
1×10^{18}	34.445519	0.8944	78.33	24.13
1×10^{19}	34.455641	0.8996	80.05	24.81
1×10^{20}	34.460774	0.9020	80.37	24.98
1×10^{21}	34.462422	0.9028	80.45	25.03

Based on the table, it is noted that the optimal N_A acceptor density for the Spiro-OMeTAD is 1×10^{21}. The short-circuit current (Jsc) increases slightly with N_A. The open-circuit voltage (Voc) shows only a slight increase with increasing N_A, and the fill factor (FF) also increases significantly, from 32.01% to 80.45% at N_A=1×10^{21} 1/cm^3 Furthermore, the overall power conversion efficiency improves with increasing N_A, ranging from 9.74% to 25.03%. Taking all these factors into account, the optimal N_A of 1×10^{21} was chosen, which represents a high efficiency of 25.03%.

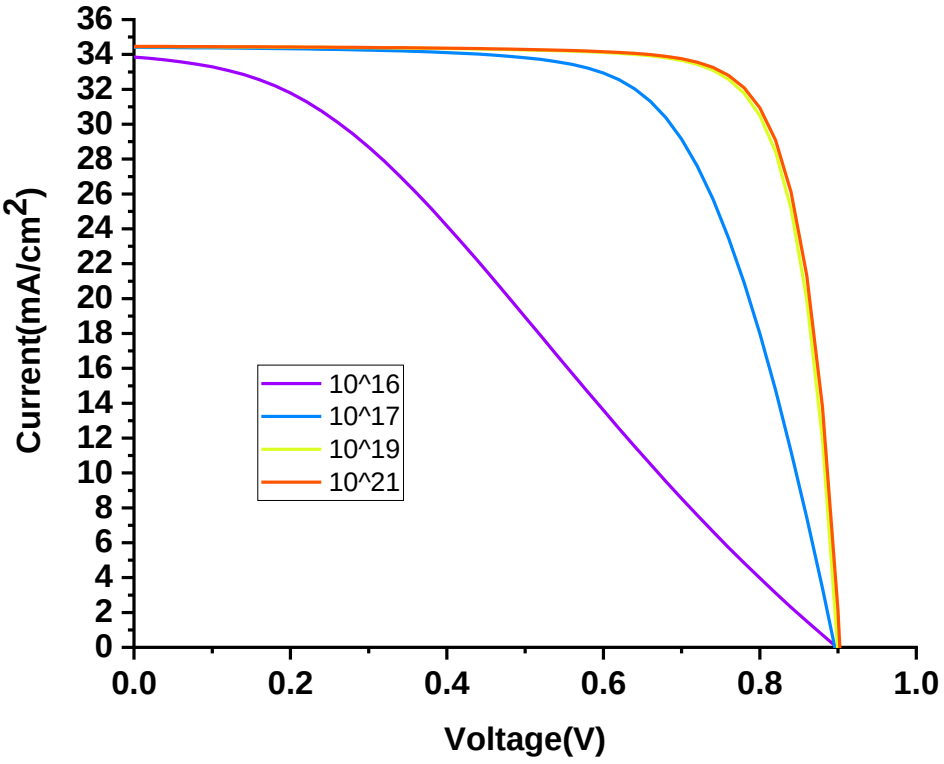

Figure IV.9 : Influence of the NA Acceptor density of the Spiro-OMeTAD layer on the J-V characteristics of the solar cell .

4.4.3. Effect of CeOx Layer Thickness on Solar Cell Photovoltaic Parameters

In our study, we varied the thickness of the ETL (CeOx) material from 0.1 to 0.5 µm. The results obtained (Jsc (mA/cm^2), V_{OC} (V), FF (%) and η (%) are shown in the following table

Table IV.6 : Effect of CeOx layer thickness on solar cell photovoltaic parameters.

thickness (µm)	$J_{sc}(\frac{mA}{cm2})$	$V_{OC}(V)$	***FF (%)***	***η (%)***
0.1	34.46242	0.9028	80.45	25.03
0.2	34.46021	0.9028	80.45	25.03
0.3	34.4575	0.9028	80.45	25.03
0.4	34.45435	0.9028	80.45	25.03
0.5	34.45083	0.9028	80.45	25.02

From this table, we note that the best CeOx layer thickness is 0.1 µm. The short-circuit current and efficiency decrease slightly with increasing thickness. The V_{OC} voltage is constant with the thickness; the same goes for the form factor, which is almost constant with increasing CeOx thickness. We chose the optimal CeOx thickness of 0.1 µm, corresponding to an efficiency of $\boldsymbol{\eta}$ = 25.03%.

Figure IV.10 shows the effect of CeOx layer thickness on the performance of the MASnI3-based perovskite solar cell.

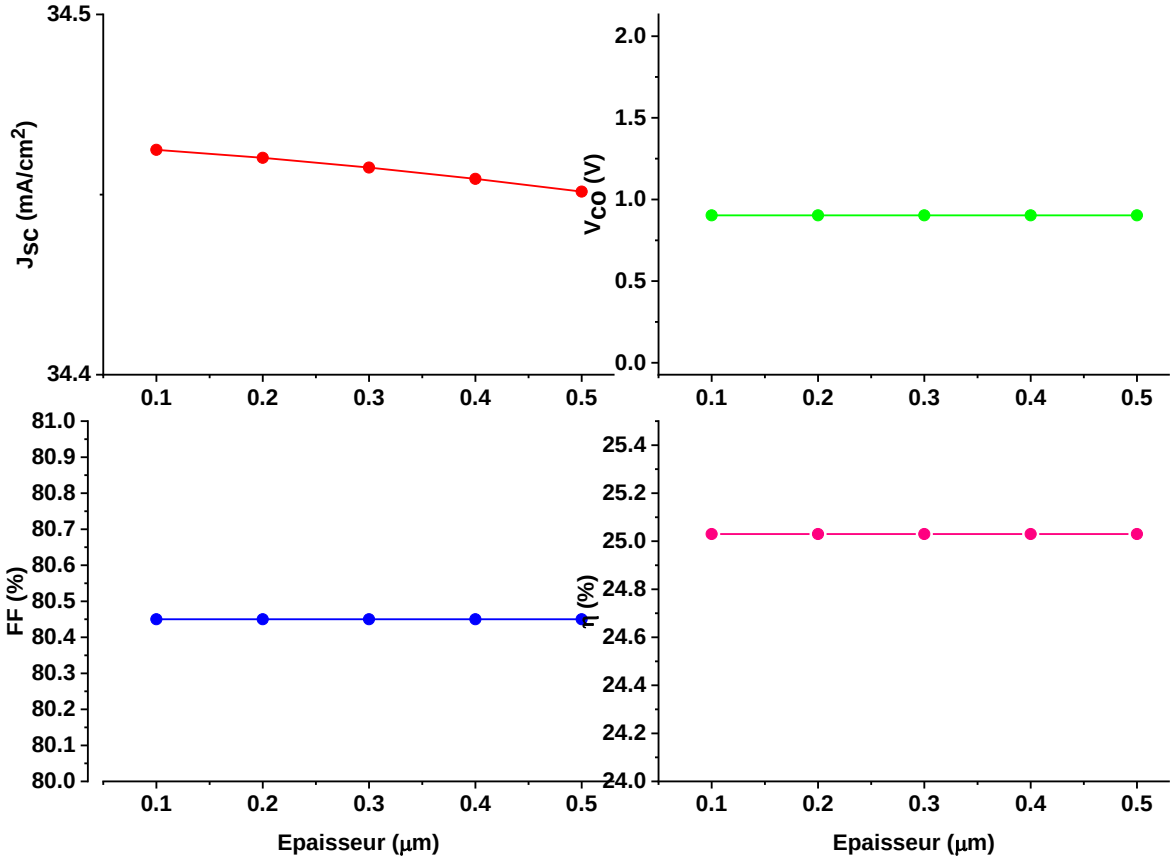

Figure IV.10 : Effect of CeOx layer thickness on solar cell photovoltaic parameters.

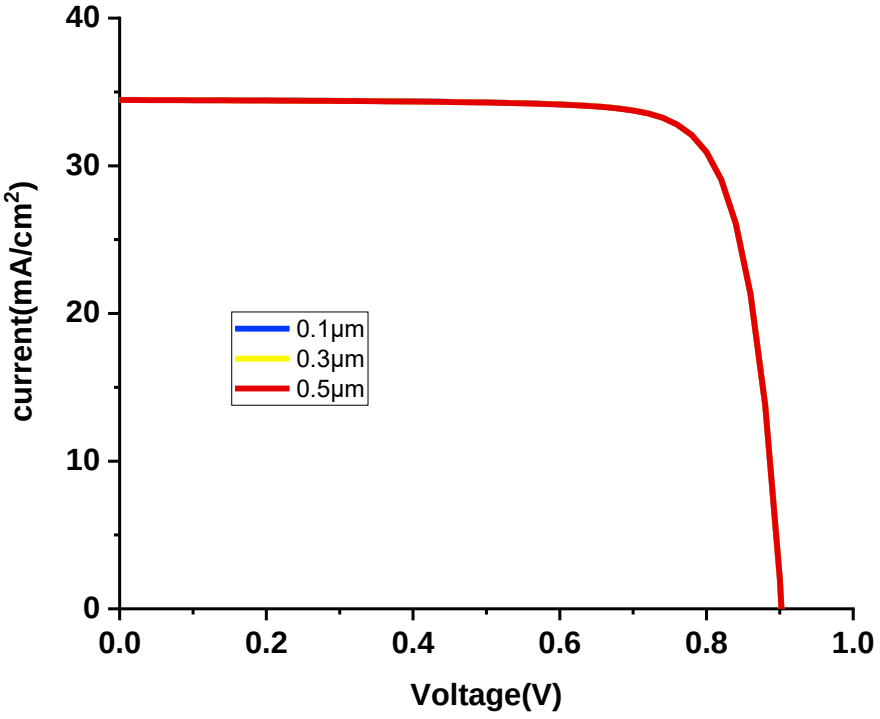

Figure IV.11 : Influence of the thickness of the CeOx layer on the J-V characteristics of the solar cell .

4.4.4. Effect of CeOx N_D Donor Density on Solar Cell Photovoltaic Parameters

In our study, we considered a perovskite layer thickness of 0.6 µm and varied the N_D Donor Density material (CeOx) from 1×10^{17} to 1×10^{21}µm. The other parameters were defined as shown in Table IV.7. The results obtained (Jsc (mA/cm²), V_{OC} (V), FF (%) and η (%)) are presented in the following table

Table IV.7 : Effect of CeOx ND Donor Density on Solar Cell Photovoltaic Parameters

ND	$J_{sc}(\frac{mA}{cm2})$	$V_{CO}(V)$	*FF (%)*	η *(%)*
1×10^{17}	34.462794	1.4276	49.30	24.25
1×10^{18}	34.466038	0.9684	72.91	24.34
1×10^{19}	34.465779	0.8957	79.97	24.69
1×10^{20}	34.464088	0.9007	80.32	24.93
1×10^{21}	34.462422	0.9028	80.45	25.03

Based on the table, it is observed that the optimal ND donor density for CeOx is 1×10^{21}. The open circuit voltage (Voc) decreases from 1.4276V to 0.9028V with

increasing N_D, and the fill factor (FF) also increases significantly, from 49.30% to 80.45% at $N_D = 1 \times 10^{21}$ 1/cm^3. Furthermore, the overall power conversion efficiency improves with increasing N_D, ranging from 24.25% to 25.03%. Considering all these factors, the optimal N_D is selected as 1×10^{21}. representing a high efficiency of 25.03%.

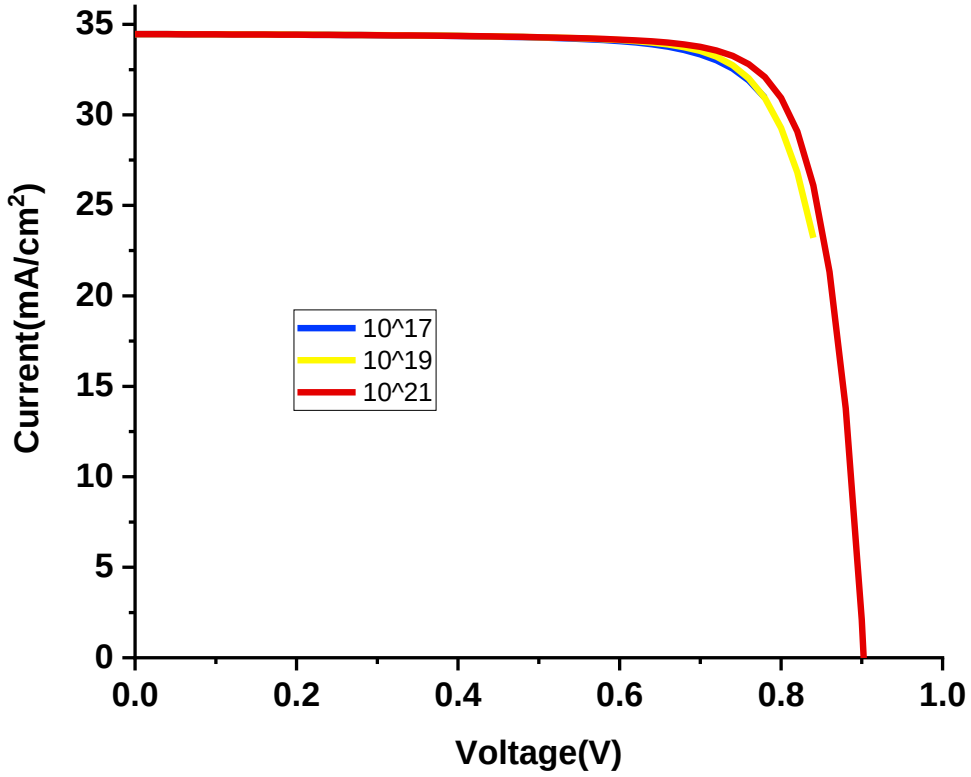

Figure IV.12 : Influence of the ND Donor density of the CeOx layer on the J-V characteristics of the solar cell .

4.4.5. Effect of TCO Layer Thickness on Solar Cell Photovoltaic Parameters

In our study, we varied the thickness of the TCO material from 0.1 to 0.5 µm. The results obtained (J_sc (mA/cm^2), V_{OC} (V), FF (%) and (%)) are shown in the following table. From this table, we note that the optimal TCO layer thickness is 0.1 µm. The short-circuit current and efficiency decrease slightly with increasing thickness. The V_{OC} voltage is constant with increasing thickness; the same goes for the form factor, which is almost constant with increasing TCO thickness. We chose the optimal TCO thickness of 0.1 µm, corresponding to an efficiency η = 25.11%.

Table IV.8 : Effect of TCO layer thickness on solar cell photovoltaic parameters.

thinckness (µm)	$J_{sc}(\frac{mA}{cm2})$	$V_{CO}(V)$	***FF (%)***	***η (%)***
0.1	34.572649	0.9029	80.45	25.11
0.2	34.539691	0.9029	80.45	25.09
0.3	34.510429	0.9028	80.45	25.07
0.4	34.484829	0.9028	80.45	25.05
0.5	34.462422	0.9028	80.45	25.03

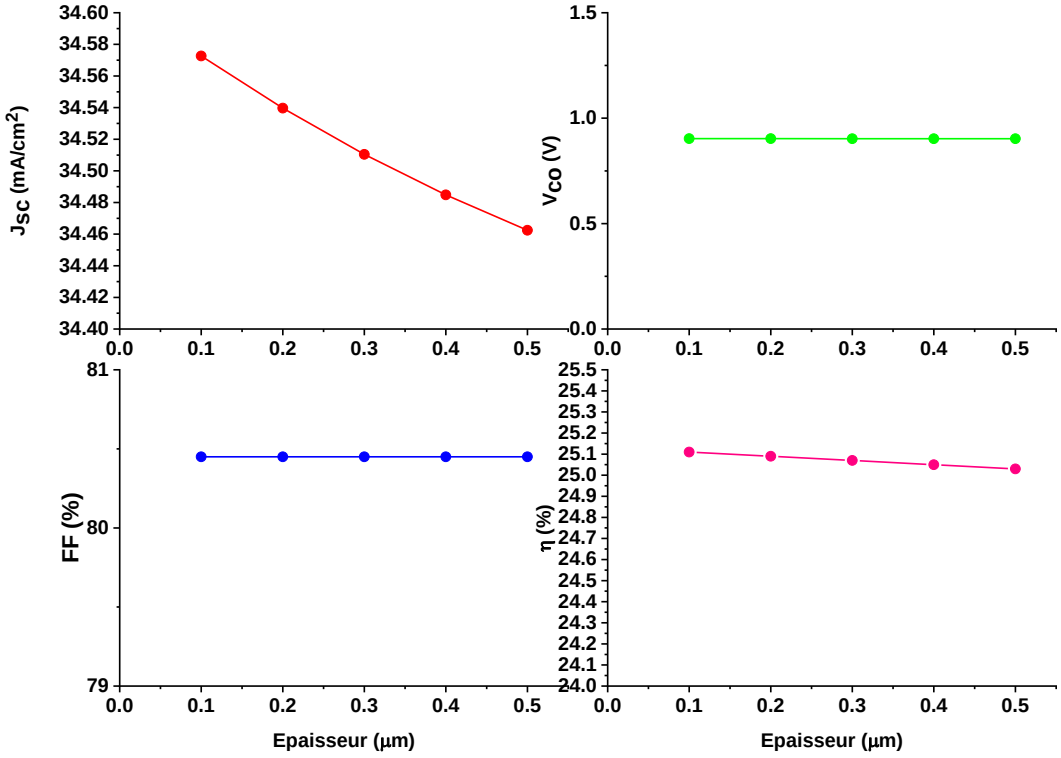

Figure IV.13 : Effect of TCO layer thickness on solar cell photovoltaic parameters.

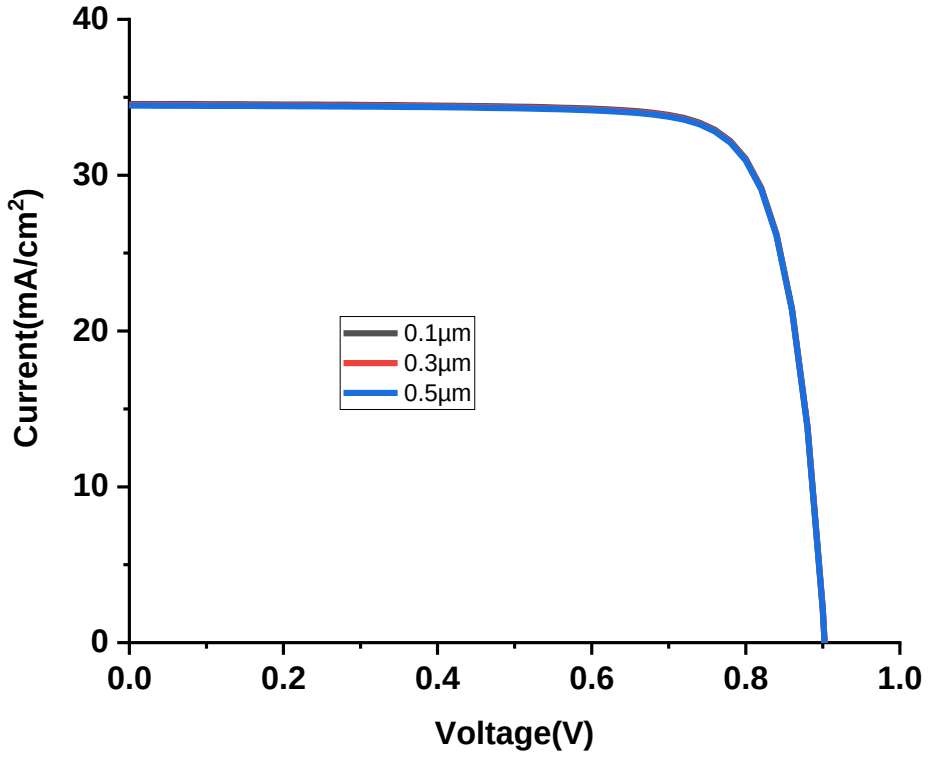

Figure IV.14 : Influence of the thickness of the TCO layer on the J-V characteristics of the solar cell

4.5. Effect of Temperature on the Solar Cell

We gradually varied the temperature of our cell, starting from 300 to 380 K. We observed a change in the photovoltaic parameters (J_{SC}(mA/cm^2),V_{OC}(V), FF(%), η(%)) illustrated in the following table

Table IV.9 : Parameters of photovoltaic solar cells as a function of temperature

temperature(°K)	$J_{sc}(\frac{mA}{cm2})$	$V_{OC}(V)$	***FF (%)***	***η (%)***
300	34.572649	0.9029	80.45	25.11
320	34.567814	0.8984	77.08	23.94
340	34.559020	0.8428	78.16	22.76
360	34.552656	0.8121	76.91	21.58
380	34.545669	0.7813	75.60	20.40

It is observed that the parameters of photovoltaic cells change with increasing temperature. The short-circuit current decreases slightly with a decrease in voltage from 0.9029 volts to

0.781 volts and also a significant decrease in FF from 80.45% to 75.60% at a temperature of 380K. In addition, the efficiency factor decreases from 25.11% to 20.40%.

Figure IV. 15 represents the effect of temperature on the photovoltaic parameters of the solar cell.

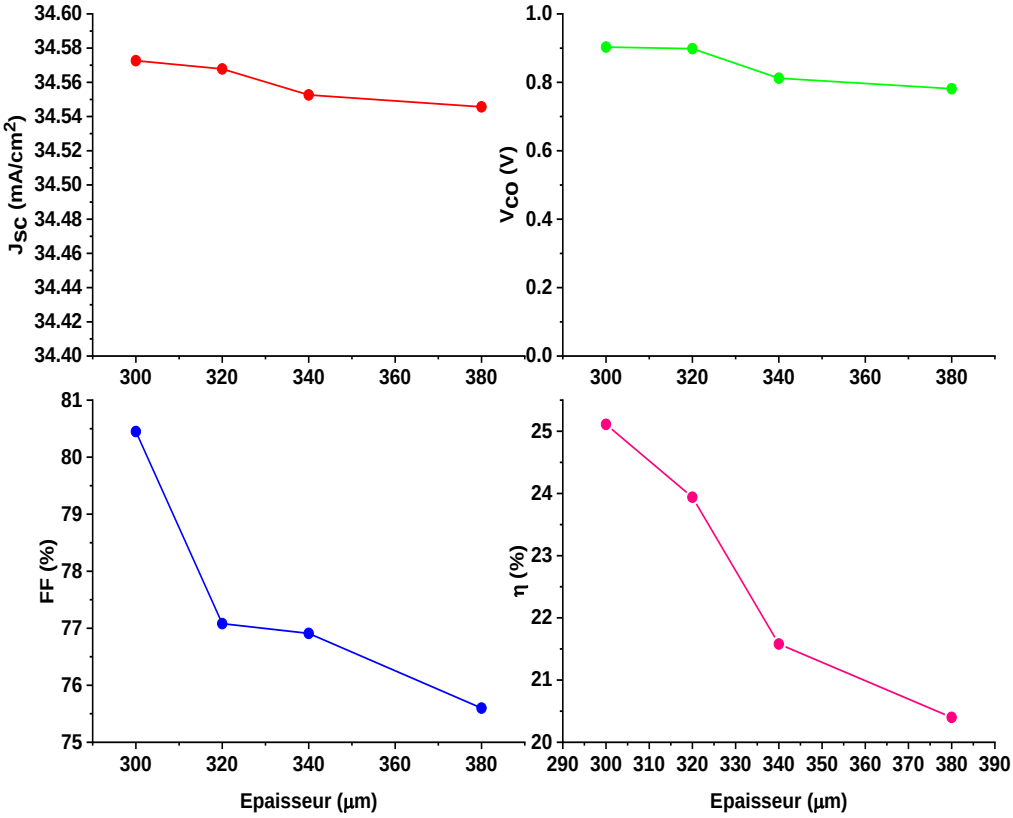

Figure IV.15 : Effect of temperature on the photovoltaic parameters of the solar cell.

This influence is also illustrated in the I-V characteristic, which is shown in Figure IV.15. We note that Vco decreases with temperature

.

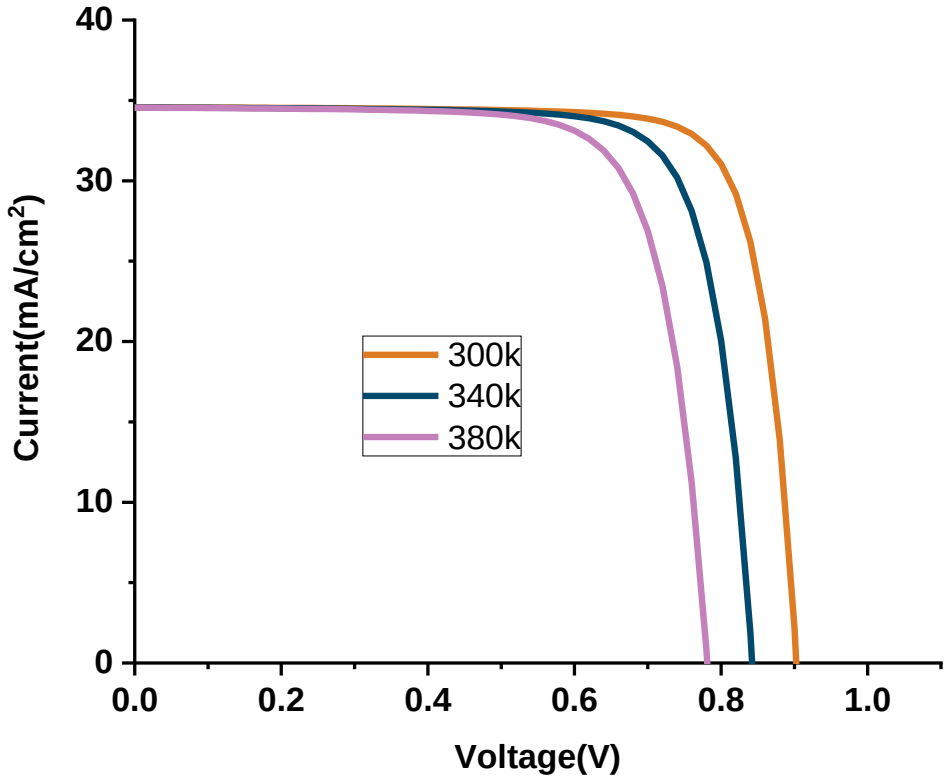

Figure IV.16 : Influence of temperature on the I-V characteristic of the solar cell

4.6. Simulation of the perovskite cell with different ETL layer materials

In our study, we simulated the ETL layer for the following materials (TiO2, ZnO, PCBM, CeOx). The results obtained were: J_{SC}(mA/cm^2),V_{OC}(V), FF (%) and η (%). The parameters of these different materials are shown in the following table [41]

Table IV.10 : Parameters of the different ETL materials.

Materials	TiO_2	ZnO	CeOx	PCMB
thickness (µm)	0.1	0.1	0.1	0.05
Bandgap (eV)	3.2	3.2	3.5	2
Electron affinity (eV)	4.26	4.26	4.3	3.9
Dielectric permittivity (relative)	9	9	9	4
CB ($1/cm^3$)	2×10^{18}	1×10^{21}	1×10^{20}	2×10^{21}
VB ($1/cm^3$)	1.8×10^{19}	2×10^{20}	2×10^{21}	1×10^{20}
Electron thermal velocity (cm/s)	1×10^{7}	1×10^{7}	1×10^{7}	1×10^{7}
hole thermal velocity (cm/s)	1×10^{7}	1×10^{7}	1×10^{7}	1×10^{7}
Electron mobility (cm^2/Vs)	0.05	200	100	1×10^{-2}
Hole mobility (cm^2/Vs)	0.05	5	2	1×10^{-2}
ND ($1/cm^3$)	6×10^{19}	1.5×10^{17}	1×10^{21}	1×10^{20}
NA ($1/cm^3$)	0	0	0	0

The results obtained (J_{sc}($mA/$ cm^2), V (V), FF (%) and $\boldsymbol{\eta}$ (%)) are shown in the following table

Table IV.11 : Photovoltaic parameters of solar cell for different ETL layer materials.

	$V_{co}(V)$	$\frac{mA}{(cm2)}$	*FF (%)*	η *(%)*
TiO_2	0.9036	34.518433	80.50	**25.11**
ZnO	0.9036	34.574096	77.87	**24.27**
PCBM	0.9004	31.808768	80.51	**23.06**
CeOx	**0.9029**	**34.572649**	**80.45**	**25.11**

From this table, we see that the best cell performance is presented by TiO2 and CeOx. The short-circuit current is beneficial for TiO2 and CeOx materials. The Vco voltage is almost constant. The form factor and efficiency are better for (TiO2, CeOx) materials and slightly lower for (PCBM, ZnO) materials.

The best ETL material is CeOx (Icc of 34.572mA/cm2, VOC of 0.9029V, FF of 80.45% and etη of 25.11%).

The influence of the different ETL layers is also illustrated on the I-V characteristic which is represented in figure IV.17

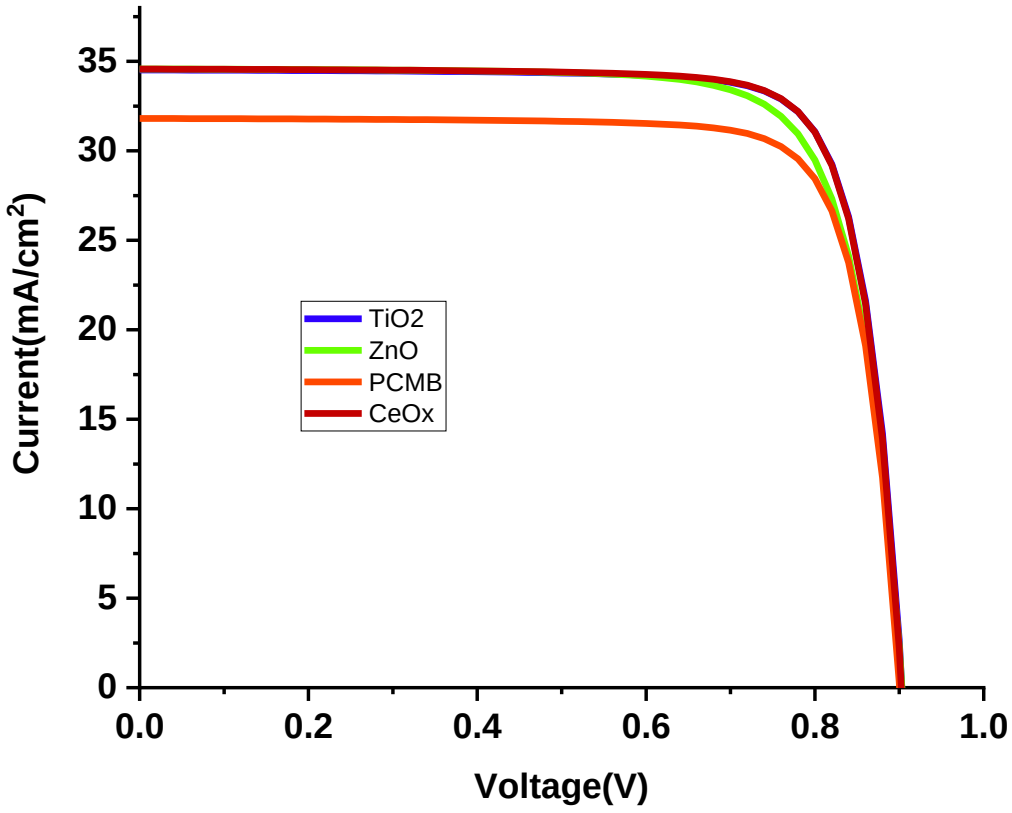

Figure IV.17 : Influence des différentes couches ETL sur la caractéristique I-V de la cellule solaire.

given that CeOx exhibits comparable efficiency to TiO_2 in the ETL layer, it can be considered a cost-effective and efficient alternative, particularly for applications requiring flexible processing or low-cost fabrication.

4.7. Effect of defect on the solar cell

In our study, we considered a perovskite layer thickness of 0.6 µm and varied the Defect1 material (MASnI3) from 1×10^{12} to 1×10^{16}1/cm^3. The other parameters were defined as shown in Table IV.12. The results obtained (Jsc (mA/cm²), V_{OC}(V), FF (%) and $\boldsymbol{\eta}$ (%)) are presented in the following table

Table IV.12 : Effect of MASnI3 defect on Solar Cell Photovoltaic Parameters

Defect	$J_{sc}(\frac{mA}{cm2})$	$V_{CO}(V)$	***FF (%)***	***η (%)***
$\mathbf{1\times 10^{12}}$	34.664084	8.0390	12.34	34.37
$\mathbf{1\times 10^{13}}$	34.663259	1.6526	56.07	32.12
$\mathbf{1\times 10^{14}}$	34.655006	1.0125	81.69	28.66
$\mathbf{1\times 10^{15}}$	34.572649	0.9029	80.45	25.11
$\mathbf{1\times 10^{16}}$	34.766175	0.8063	71.45	19.4

Based on the table, it is noted that the optimal defect value for MASnI3 is 1×10^{14} 1/cm^3. The open-circuit voltage decreases from 8.039V to 0.8063 V with increasing defect, and the fill factor (FF) increases significantly from 12.34% to 81.69% at defect =1×10^{14} 1/cm^3 Then it decreases after that. Furthermore, the overall power conversion efficiency decreases with increasing defect, ranging from 19.47% to 34.37%. Based on these factors, the optimal defect value is chosen to be1×10^{14} 1/cm^3,representing a high efficiency of 28.66%. The FF is 81.69%.

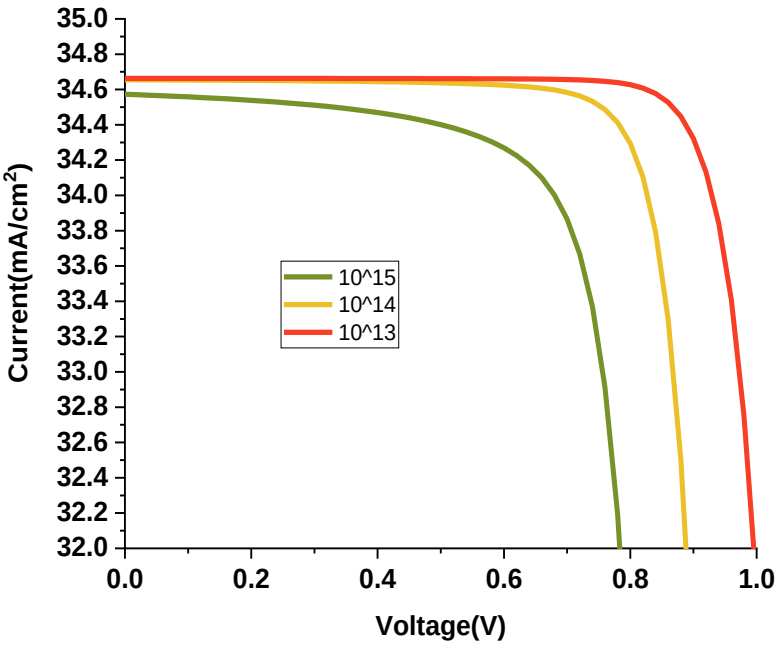

Figure IV.18 : Influence of Defect on the I-V characteristic of the solar cell.

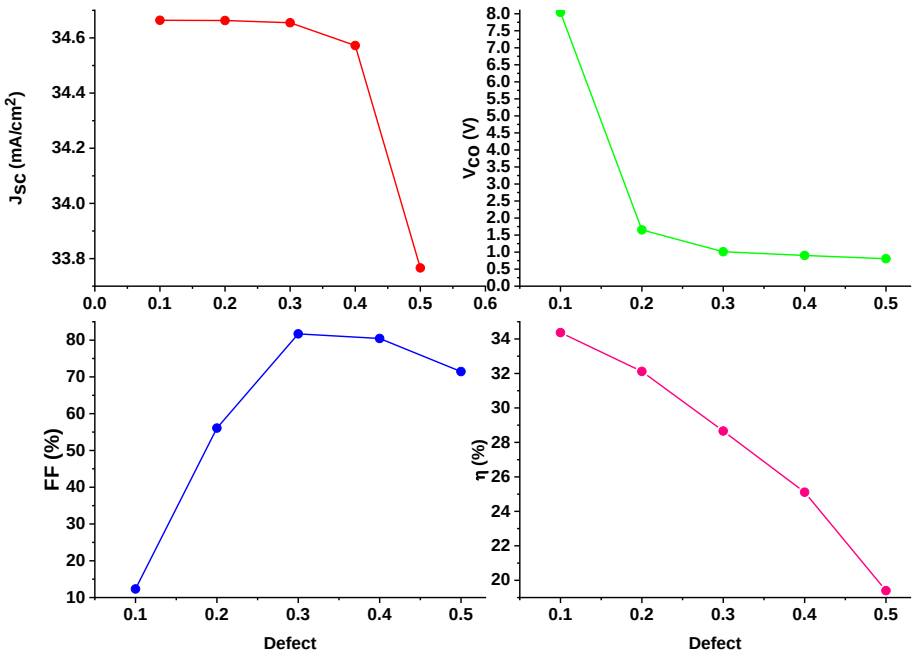

Figure IV.19 : Effect of Defect on the photovoltaic parameters of the solar cell

4.8. Effects of (Spiro-OMeTAD/MASnI3) and (MASnI3/Ceox) Interface Defects

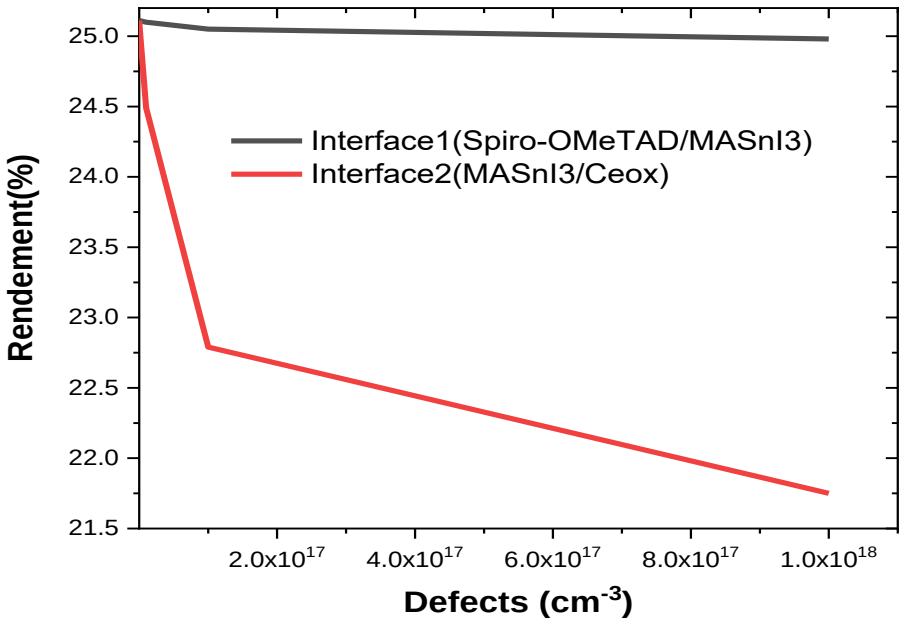

Figure IV.20 : Solar cell electrical efficiency as a function of(Spiro-OMeTAD/MASnI3) and (MASnI3/Ceox) interface defect densities.

From Figure IV.20, we can conclude the influence of interface defects on the electrical efficiency of our solar cell.

For (Spiro-OMeTAD/MASnI3) interface defect densities ranging from 1.00E+10 to 1.00E+18, we recorded a slight decrease in efficiency from 25.11% to 24.98%. However, for the same range of (MASnI3/Ceox) interface defect densities, we recorded a significant decrease from 25.11% to 21.75%.

4.9. Conclusion

Through the study we conducted in this unit, we improved the solar cell based on MASnI3 with the structure: Spiro-OMeTAD /MASnI3/CeOx/TCO.

- The perovskite MASnI3 has a thickness of 0.6 µm.
- The Spiro-OMeTAD has a thickness of 0.1 µm.
- The CeOx a layer also has thickness of 0.1 µm.
- The TCO layer has a thickness of 0.1 µm.
- Additionally, the N_A in the Spiro-OMeTAD layer is 1×10^{21}1/cm^{3}and the N_D of CeOx layer is also , 1×10^{21} 1/cm^3, which was found to be optimal.

After studying various materials from ETL, we found that CeOx is a good and a competitive alternative to TiO2.

General Conclusion

GENERAL CONCLUSION

In this work, we simulated a solar cell based on the hybrid perovskite material $MASnI_3$ using the one-dimensional solar cell simulation software SCAPS. The device structure consists of the following layers**:** CeOx as the electron transport layer (ETL**),** $MASnI_3$ as the absorber layer, and Spiro-OMeTAD as the hole transport layer (HTL).

We began by optimizing the thicknesses of these three layers to enhance the overall performance of the solar cell. Additionally, we studied the influence of the donor concentration (N_D) in the CeOx layer and the acceptor concentration (N_A) in the Spiro-OMeTAD layer. We also investigated the impact of interface defects and bulk defects in the perovskite absorber layer**.**

The results showed that the optimal device configuration Spiro-OMeTAD / $MASnI_3$ / CeOx / TCO provides the best photovoltaic performance with the following values:

- ✓ The perovskite layer of MASnI3 with a thickness of 0.6 μm gives the following photovoltaic parameters: short-circuit current Jsc = 34.4556 mA/cm^2, Voc = 0.8996 , FF = 80.05% and η = 24.81 %
- ✓ The Spiro-MeOTAD layer with a thickness of 0.1 μm gives the following photovoltaic parameters: Jsc = 34.4556 mA/cm2, Voc = 0.8996 , FF = 80.05% and η = 24.81%.
- ✓ The Spiro-MeOTAD layer with a N_A of 10^{21} cm^{-3} gives the following photovoltaic parameters: Jsc = 34.4624 mA/cm2, Voc = 0.9028 V , FF = 80.45% and η = 25.03%.
- ✓ The CeOx layer with a thickness of 0.1μm gives the following photovoltaic parameters: Jsc = 34.4624 mA/cm2, Voc = 0.9028 V, FF = 80.45% and η = 25.03%.

- ✓ The CeOx layer with a N_D of 10^{21} cm^{-3} gives the following photovoltaic parameters: Jsc = 34.4624 mA/cm2, Voc = 0.9028 V , FF = 80.45% and η = 25.03%.
- ✓ The TCO layer with a thickness of 0.1 μm gives the following photovoltaic parameters: Jsc = 34.5726 mA/cm2, Voc = 0.9029 , FF = 80.45% and η = 25.11%.

A comparison between different ETL materials showed that CeOx and TiO_2 exhibit nearly identical performance. Therefore, CeOx can be considered a good low-cost alternative.

The temperature analysis revealed that the cell efficiency decreases with increasing temperature, emphasizing the importance of considering thermal operating conditions when designing this type of solar cell.

Finally, lower densities of defects in the perovskite layer and at interfaces lead to enhanced solar cell performance, as it reduces non-radiative recombination losses and improves charge carrier transport.

Future Outlook

Tin-based perovskite solar cells such as $MASnI_3$ are expected to gain significant attention as environmentally friendly alternatives to lead-based cells, due to their non-toxicity and potential for high performance.

Simulation tools like SCAPS-1D will continue to play a key role in solar cell research, enabling cost-effective, time-saving, and highly accurate analysis of materials and device structures before physical fabrication.

If issues related to chemical and thermal stability are resolved, $MASnI_3$-based cells could be integrated into real-world applications, including wearable devices, self-powered sensors, building-integrated photovoltaics (BIPV), and off-grid systems.

Future research may extend this study by investigating the impact of alternative transport layers (HTL/ETL), advanced multilayer architectures, and interface engineering to further boost device performance.

$MASnI_3$ has shown promising results in terms of high optical absorption, tunable bandgap, and compatibility with low-cost fabrication methods, making it an attractive candidate for next-generation solar technologies.

In addition, combining $MASnI_3$ with nanostructured or 2D materials could enhance charge transport and stability, opening new paths in the development of flexible and lightweight solar cells.

This study provides a solid foundation for experimental validation and industrial-scale research, contributing to the global shift toward clean and sustainable energy.

References

References

[1] B. MHENNA et G. FERHAT, « Alimentation d'un moteur à courant continu par une source photovoltaïque », mémoire de master académique. Université Mouloud Mammeri de TIZI OUZOU, 2018.

[2] « The Solar RadiationSpectr_ThanhTran -Introduction to Solar Radiation p 17 ».

[3] « M. Dankassoua, S. Madougou, et A. Aboubacar, « Etude du rayonnement solaire global à Niamey de la période de pré-mousson et de la mousson de l'année 2013 (mai à octobre) », p. 16, Vol. 20 N°1 ,2017» .

[4] https://www.futura-sciences.com/sciences/definitions/physique-longueur-onde-4575/

[5] L. Bekhouche, H. Haftari: « Synthèse sur les cellules solaire à base de silicium », Mémoire de Master, Université Abbas Laghrour de Khanchela, (2011).

[6] J.XUEYANG, "Étude comparative de structures de convertisseurs pour les systèmes photovoltaiques connectés à un réseau électrique moyenne tension," 2019.

[7] M. A. Slimani, "Cellules solaires pérovskites imprimées et optimisation des couches pérovskites pour les cellules tandems," 2019.

[8] BENRABBAH, Rafik. *Développement de procédés plasma pour l'élaboration et la caractérisation du silicium photovoltaïque: dépôt de couches minces épitaxiées de silicium par PECVD: mesure de la pureté du silicium à l'état solide (20° C) et liquide (1414° C) par LIBS*. 2015. Thèse de doctorat. Université Pierre et Marie Curie-Paris VI.

[9] "L'énergie photovoltaïque et les cellules solaires". Available: https://nanopdf.com/ download/chapitre-i-lenergie-photovoltaque-et-les-cellules-solaires_pdf

[10] "Production d'énergie électrique: Energie_solaire_photovoltaique". Available: https://www.doc-developpement-durable.org/file/Energie/Solaire-photovolta%C3% AFque/Energie_solaire_photovoltaique.pdf.

[11] M. Habibi, F. Zabihi, M. R. Ahmadian-Yazdi et M. Eslamian, « Progress in cellules solaires émergentes à couche mince traitées en solution – Partie II : cellules solaires à pérovskite, » Revues des énergies renouvelables et durables, vol. 62, pages 1012-1031, 2016.

[12] Henry Mathieu-Hervé Fanet « Physique des semi-conducteurs et des composants électroniques » 6ème édition.

[13] OUDDAH MOURAD « Étude du silicium poreux destine aux cellules solaires », Mémoire de magister, Université Mentouri – Constantine, 2009.

[14] K. TAKI EDDINE, « Modélisation et commande d'un système photovoltaïque connecté au réseau électrique », mémoire de master. Université MOHAMED BOUDIAF M'SILA, 2016.

[15] M. Naïma TOUAFEK, « Contribution à l'étude d'une cellule solaire en couches minces à base de CuIn1-xGaxSe2 », Thèse de Doctorat, Université Mentouri – Constantine, 2015.

[16] S.M. Sze, 'Physics of Semiconductors Devices', A. Wiley, Interscience Publication, New York, 1981.

[17] Angel Cid Pastor. « Conception et réalisation de modules photovoltaïques électroniques ». Thèse de doctorat, Institut National des Sciences Appliquées de Toulouse, France. 2006.

[18] Zahra, Meziani. « Modelisation de modules photovoltaiques». Universite de Batna,

Faculte de Technologie, Département d9Electronique, 2012.

[19] « Z. El Jouad, "Réalisation et caractérisation des cellules photovoltaïques organiques," PhDThesis, Université d'Angers, p108,2016 ».

[20] «V. V. Tyagi, N. A. A. Rahim, N. A. Rahim, et J. A. /L. Selvaraj," Progress in solar PV technology: Research and achievement ", vol. 20, p. 443-461, avr. 2013»

[21] BENNAOUM Menouer, THESE DE DOCTORAT ' Etude Théorique des Cellules Solaires à base de Pérovskite', UNIVERSITE DJILLALI LIABES FACULTE DE GENIE ELECTRIQUE SIDI BEL ABBES.

[22] Sara CHERIFI, Mohamed HADDAD, « L'ÉNERGIE SOLAIRE : UN MOTEUR DU DÉVELOPPEMENT DURABLE EN ALGÉRIE », Les Cahiers du Cread, vol. 35 - n° 03 – 2019, Laboratoire de la mondialisation et des politiques économiques, Université d'Alger3.

[23] Energies Nouvelles, Renouvelables et Maitrise de l'Energie, Ministère de l'énergie et des mines de la République Algérienne, https://www.energy.gov.dz/?rubrique=energiesnouvelles-renouvelables-et-maitrise-de-lrenergie

[24] ZHOU, Chenkun, LIN, Haoran, HE, Qingquan, et al. Low dimensional metal halide perovskites and hybrids. Materials Science and Engineering: R: Reports, 2019, vol. 137, p. 38-65.

[25] DIAB, Hiba. Propriétés optiques des pérovskites hybrides 3D pour le photovoltaique. 2017. Thèse de doctorat. Université Paris-Saclay.

[26] MITZI, David B., CHONDROUDIS, Konstantinos, et KAGAN, Cherie R. Organic-inorganic electronics. IBM journal of research and development, 2001, vol. 45, no 1, p. 29-45.

[27] Pia Dally. Cellules Solaires à base de Matériaux Pérovskites : De la caractérisation des matériaux à l'amélioration des rendements et de la stabilité. Génie des procédés. Université Grenoble Alpes, 2019. Français. NNT : 2019GREAI093. tel-02499789.

[28] BERRY, Florian. Nanostructuration et cristaux photoniques à base de pérovskites hybrides pour applications photovoltaïques. 2020. Thèse de doctorat. Université de lyon.

[29] Article « Les cellules solaires à base de matériaux pérovskites - Structures et performances » O. Ourahmoun * Laboratoire des Technologies Avancée, LATAGE,Faculté de Génie Electrique et d'Informatique, Université Mouloud Mammeri de Tizi-Ouzou, UMMTO, B.P. N°17 15000, Tizi-Ouzou, Algérie. Revue des Energies Renouvelables Vol. 21 N°4 (2018) 515 – 520.

[30] Laid KADRI. Thèse de doctorat université Oran Mohamed Boudiafe 'Etude, synthèse et optimisation de la couche compacte de TiO2 pour applications cellules solaires'.

[31] P. Edelman, W. Henley et J. Lagowski, « Imagerie de longueur de diffusion de photoluminescence et de porteurs minoritaires dans le silicium et le GaAs », Semicond. Sci. Technol., Vol. 7, non. 1A, p. A22 – A26, janvier 1992

[32] He, D., Chen, P., Wang, L., et al. (2025). Hétérostructures homogènes 2D/3D dans *les* photovoltaïques à pérovskites à halogénure d'étain**.** Nature Nanotechnology

[33] BEN SAOUCHA, Zine laabidine, et DJEHICHE, Badereddine. Simulation numérique de la cellule solaire Tandem Pérovskite/CIGS. Mémoire de master. 2019/2020. Université Mohamed Boudiaf-M'Sila.

[34] BOUDEA, Wissam. Les propriétés structurales et é lectroniques du chlorure pérovskite CsCdCl 3. 2020. Thèse de doctorat. Université Mohamed Boudiaf-M'Sila

[35] T.R. Shrout, A. Halliyal, «Preparation of lead-based ferroelectric rellaxors for capacitors ». Am. Ceram. Soc. Bull, 66 (1987) 704 -711.

[36] Shen Wang. Function of Hole Transport Layer Componentsin Perovskite Solar Cells,A dissertation submitted in partial satisfaction of therequirements for the degree Doctor of Philosophy in NanoEngineering 2018. UNIVERSITY OF CALIFORNIA SANDIEGO.

[37] YANGUI, Aymen. Etude des propriétés optiques et structurales des matériaux hybrides organiques-inorganiques à base de Plomb: émission de lumière blanche. 2016. Thèse de doctorat. Université Paris-Saclay (ComUE).

[38] GOUFI Meriem &HAMDOUNI Badr « Etude et Simulation D'une Cellule Photovoltaïque à Pérovskite **»**. Université Larbi Ben M'Hidi O.E.B.

[39] ZOUARI AHMED Mammar & SLIMANI Abdelhamid, MASTER ACADEMIQUE, « Simulation Et Optimisation D'une Cellule Solaire A Base Du Pérovskite CH3NH3SnI3 En Architecture NIP », Université Echahid Hamma Lakhdar D'El-Oued.

[40] Al-Mousoi, A. K., Mohammed, M. K. A., Pandey, R., Madan, J., Dastan, D., Ravi, G., Sakthivel, P., & Anandha Babu, G. (2022). Simulation and analysis of lead-free perovskite solar cells incorporating cerium oxide as electron transporting layer. RSC Advances, 12, 32365–32373.

[41] K. Deepthi Jayan , Varkey Sebastian, Comprehensive device modeling and performance analysis of $MASnI_3$ based peroviskite solar cells with diverse ETM, HTM and back metal contacts. Departement of Physics, Nirmalagiri College, Kannur University, Kannur, kerala 670701 , India